# Dease Lake Geoscience Project: Geochemical Characteristics of Tsaybahe, Stuhini and Hazelton Volcanic Rocks, Northwestern British Columbia (NTS 104I, J)

**J.M. Logan,** **British Columbia Ministry of Energy, Mines and Natural Gas, Victoria, BC, Jim.Logan@gov.bc.ca**

**O. Iverson,** **University of Wisconsin, Eau Claire, WI**

Logan, J.M. and Iverson, O. (2013): Dease Lake Geoscience Project: geochemical characteristics of Tsaybahe, Stuhini and Hazelton volcanic rocks, northwestern British Columbia (NTS 104I, J); *in* Geoscience BC Summary of Activities 2012, Geoscience BC, Report 2013-1, p. 11–32.

## Introduction

The BC Geological Survey's Dease Lake Geoscience Project was part of Geoscience BC's QUEST-Northwest initiative, a program launched in 2011 to stimulate exploration in the northwestern part of the province along Highway 37 (Figure 1). In 2011, the BC Geological Survey completed four field-based studies located within a 70 km radius of the Dease Lake community (Logan et al., 2012a, Figure 1b). These studies investigated regional aspects of stratigraphy, magmatic evolution and metallogeny along part of the Stikine arch, within the broader footprint of the QUEST-Northwest airborne geophysical survey (Simpson, 2012). They included regional bedrock mapping of the Dease Lake and Little Tuya River map areas (Logan et al., 2012b, c); detailed studies of the ages, emplacement history and mineralization of the Hotailuh batholith (van Straaten et al., 2012a, b) and Snow Peak pluton (Moynihan and Logan, 2012); and a lithological and geochemical characterization of the Middle Triassic Tsaybahe Group (Iverson et al., 2012a).

The Dease Lake study area is situated within the Stikine terrane, an extensive subduction-generated island arc magmatic complex that includes Late Triassic and Early Jurassic calcalkaline and alkaline plutons that are associated with significant Cu-Au mineralization. Calcalkaline and alkaline Cu-Au porphyry deposits in Stikinia are hosted in thick successions of Late Triassic to Early Jurassic(?) volcanic rocks and comagmatic calcalkaline (Scott et al., 2008) and alkaline plutons (Barr et al., 1976; Lueck and Russell, 1994). The deposits are localized along parallel linear belts within high(?) level magmatic centres characterized by zones of brecciation and alkali-rich hydrothermal alteration. The volcanic stratigraphy adjacent to magmatic centres often records the evolution of magmatism

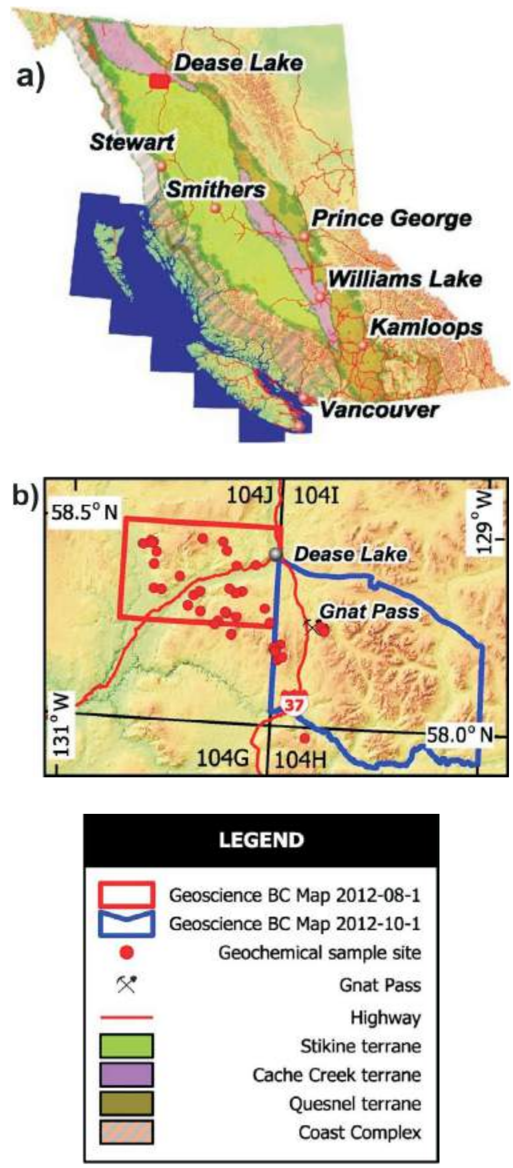


**Figure 1.** Location of the QUEST-Northwest Mapping–BC Geological Survey Dease Lake Geoscience Project on the **a)** British Columbia terrane map (after Massey et al., 2005); detailed view **b)** straddles the area covered by the Dease Lake (NTS 104J) and Cry Lake (NTS 104I) 1:250 000 map sheets at Dease Lake, and shows the locations of Geoscience BC Map 2012-08-1, Geoscience BC Map 2012-10-1 and the sample locations for the geochemistry study discussed in this paper.

***Keywords**: QUEST-Northwest mapping, regional bedrock mapping, integrated multidisciplinary studies, geochemistry, Stikine terrane, Triassic–Jurassic magmatism, Tsaybahe, Stuhini, Hazelton, Hotailuh*

*This publication is also available, free of charge, as colour digital files in Adobe Acrobat® PDF format from the Geoscience BC website: http://www.geosciencebc.com/s/DataReleases.asp.*

through changes in mineralogy (pyroxene, hornblende or plagioclase porphyry flows) and chemistry (i.e., alkali-rich stratigraphy), or through the presence of mineralized subvolcanic clasts—all of which can provide vectors to guide exploration for Cu-Au mineralization (Fox, 1975; Allen et al., 1976; Panteleyev et al., 1996, Logan and Bath, 2006).

In this paper major, trace and rare earth element chemical characteristics of volcanic rocks collected during the 2011 programs, carried out by the BC Geological Survey in the area of the Dease Lake (104J) and Cry Lake (104I) map sheets (Figure 1), are presented. Volcanic rocks were collected from the Middle Triassic Tsaybahe Group to characterize the initiation of Triassic arc magmatism and from the Late Triassic Stuhini Group to characterize its ongoing evolution, which periodically culminated in porphyry Cu–Au±Mo mineralization (i.e., Schaft Creek, Galore Creek and Red Chris deposits). A third suite comprises samples collected from a Early to Middle Jurassic volcanic and sedimentary succession, assigned to the Hazelton Group, that is the same age as the host rocks at the Eskay Creek gold mine (Alldrick et al., 2004).

## Regional Stratigraphy

The area covered by the Dease Lake and Cry Lake map sheets (NTS 104J and I, Figure 1) straddles the boundary between the Cache Creek and Stikine terranes, marked by the early Middle Jurassic south-directed King Salmon thrust fault (Gabrielse, 1998). At this latitude the Stikine terrane is composed of three overlapping island arc successions, spanning 200 m.y. from Devonian to Middle Jurassic, and is represented by volcanic and sedimentary rocks of the Paleozoic Stikine assemblage, the Triassic Tsaybahe/ Stuhini Group and the Jurassic Hazelton Group. Arc-related plutonic rocks include the Devonian-Carboniferous Forrest Kerr suite, the Late Triassic Stikine and Copper Mountain suites, the Early Jurassic Texas Creek suite and the Middle Jurassic Three Sisters suite (Anderson, 1983, 1993; Woodsworth et al., 1991; Brown et al., 1996; Logan et al., 2000). These plutonic suites are best exposed along the Stikine arch, an east-trending area of uplifted Jurassic and older rocks that bound the northern margin of the Bowser Basin. Long-lived arc magmatism in the Stikine arch has produced diverse styles of magmatism (calcalkaline and alkaline) and large Cu–Au–Ag±Mo mineral deposits associated with some intrusive centres (i.e., Snip, Galore Creek, Schaft Creek and Kemess).

The oldest Stikine rocks in the study area are Early Permian limestone, phyllite, chert and metavolcanic rocks exposed in north to northeasterly trending structural culminations. Volcaniclastic beds and coarse pyroxene-phyric basalt breccias unconformably overlie these foliated late Paleozoic rocks (Figure 2) and correlate with Early and Middle Triassic cherty sedimentary rocks and pyroxene-phyric breccias of the Tsaybahe Group to the south (Read, 1983, 1984). The green augite porphyry volcanic rocks that characterize the type section at Tsaybahe Mountain (Read and Psutka, 1990) are not easily distinguished from the younger Stuhini Group rocks and, as a result, Gabrielse (1998) included the Tsaybahe rocks as a unit within the Stuhini Group, and considered this group to encompass all Triassic volcanic and related sedimentary rocks in Stikinia. For lithogeochemical comparison in this study, the term Tsaybahe Group has been retained for all the pre–Late Triassic crowded-augite–phyric basalt overlying Paleozoic rocks (Logan et al., 2012c).

The Tsaybahe Group basalt breccias in the Dease Lake area (Gabrielse, 1998; Logan et al., 2012c) dip north below a pile of Late Triassic Stuhini Group arc rocks ~2050 m thick, comprised of pyroxene-rich volcaniclastic rocks and rare pyroxene-phyric, plagioclase-phyric and aphyric basalt flows that generally fine upward into a stratigraphic section that is dominated by unstratified coarse volcaniclastic deposits. The Stuhini volcaniclastic strata are pyroxene- and plagioclase-crystal–rich matrix-supported boulder to granule conglomerates dominated by pyroxene±plagioclase porphyry clasts with lithic arenites and rare well-bedded siltstone. The uppermost unit of the Stuhini Group comprises volcaniclastic rocks and basalt flows, and is unconformably(?) overlain by Early Jurassic Takwahoni Formation quartz-bearing conglomerate and sandstone (Figure 2) of the Whitehorse Trough.

Marsden and Thorkelson (1992) include all Early and Middle Jurassic volcanic and related sedimentary rocks of Stikinia in the Hazelton Group. As a result, the Hazelton Group includes a wide variety of rock types that formed in diverse volcanic environments over a large region. The Hazelton Group in northern Stikinia overlies Late Triassic calcalkaline and alkaline volcanic and sedimentary rocks of the Stuhini Group and associated arc plutonic rocks, and is overlain by Middle Jurassic sedimentary rocks of the Bowser Lake Group.

Southeast of the study area, in the area covered by the Spatsizi River map sheet (104H), Late Triassic Griffith Creek volcanic rocks, Early Jurassic Cold Fish and Mount Brock volcanic rocks, and Middle Jurassic Spatsizi sedimentary rocks comprise the Hazelton Group (Evenchick and Thorkelson, 2005). Brown et al. (1992) describe a Toarcian to Aalenian calcalkaline volcanic and sedimentary succession of Hazelton Group rocks at Cone Mountain, 125 km southwest of Dease Lake within the area covered by the Telegraph Creek map sheet (104G). Like the section east of Gnat Pass (this study), the lower unit contains an abundant fauna that suggest a Toarcian age, but rather than unconformably overlying intrusive rocks of the Late Triassic Cake Hill Pluton (Henderson and Perry,

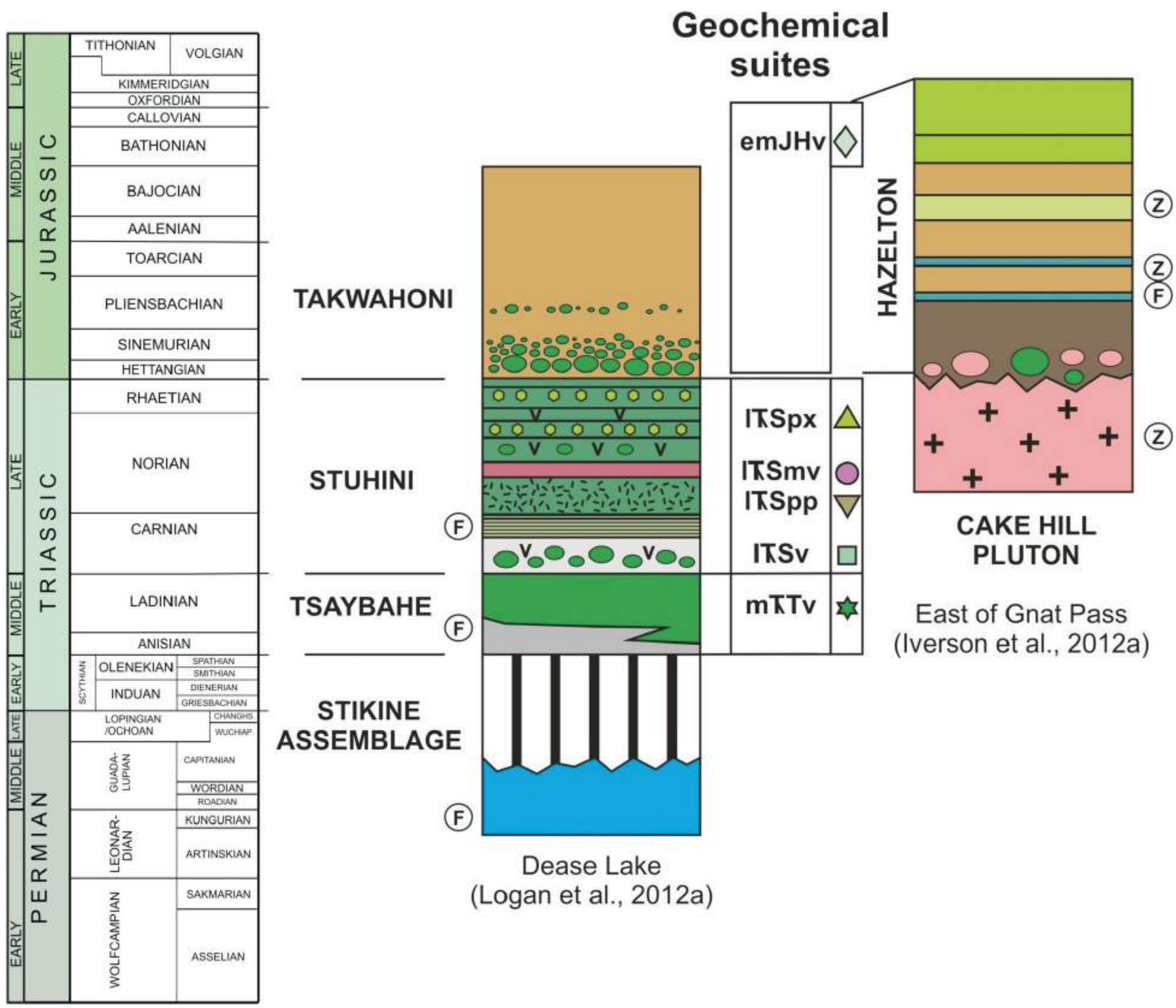


**Figure 2**. Two schematic sections illustrating the stratigraphic and plutonic relationships for Stikine terrane rocks in the study area. Abbreviations: F, fossils; Z, U/Pb zircon ages described and referenced in text. Symbols for the six geochemical suites discussed in text: mTTv, Middle Triassic Tsaybahe pyroxene-phyric basalt; lTSv, Late Triassic Stuhini aphyric basalts; lTSpp, Late Triassic Stuhini plagioclase-phyric basalt and andesite; lTSmv, Late Triassic Stuhini latite porphyry; lTSpx, Late Triassic Stuhini pyroxene-phyric basalt; emJHv, Early to Middle Jurassic Hazelton pyroxene porphyry.

1980), it overlies folded and faulted late Norian Stuhini Group strata (Brown et al., 1992).

Southeast of Dease Lake and 5 km east of Gnat Pass, is a well exposed, upright section of Early to Middle Jurassic sedimentary and volcanic rocks (Iverson, et al., 2012a) that nonconformably overly Late Triassic quartz monzonite of the Cake Hill pluton (Anderson, 1983; Gabrielse, 1998; Figure 2). Coarse pyroxene-phyric basalt breccia and volcanic conglomerate comprise the upper part of the section, which has been dated as Toarcian using fossils (Henderson and Perry, 1981), but is possibly as young as Bajocian, as dated with detrital zircons (Iverson et al., 2012a, b). The volcanic rocks are included in the Hazelton Group because of their age, but are lithologically similar to pyroxene-phyric basalt breccias of the Middle Triassic Tsaybahe and Late Triassic Stuhini groups.

## Lithogeochemistry

### Analytical Techniques

A total of 55 least-altered lithogeochemical samples were collected: 42 volcanic rocks from 5 different units and 13 intrusive rocks from 5 plutonic suites (Table 1). This paper focuses on the geochemical results of the Tsaybahe, Stuhini and Hazelton groups (n=39). The samples were jaw crushed at the BC Geological Survey sample preparation facilities in Victoria. The crushed samples were sent to Activation Laboratories in Ancaster (Ontario), where they

**Table 1. Part I:** Major oxide analytical results for volcanic and intrusive rocks collected from the area covered by the Dease Lake (104J) and Cry Lake (104I) map sheets, northern British Columbia.

| Sample numbers | | Sample location[1] | | | Analyte Symbol: | $SiO_2$ | $Al_2O_3$ | $Fe_2O_3^{(T)}$ | MnO | MgO | CaO | $Na_2O$ | $K_2O$ | $TiO_2$ | $P_2O_5$ | LOI | Total |
|---|---|---|---|---|---|---|---|---|---|---|---|---|---|---|---|---|---|
| | | | | | Unit: | % | % | % | % | % | % | % | % | % | % | % | % |
| | | | | | Detection limit: | 0.01 | 0.01 | 0.01 | 0.001 | 0.01 | 0.01 | 0.01 | 0.01 | 0.001 | 0.01 | | 0.01 |
| Geochemical | Original | Easting | Northing | Unit[5] | Sample description | | | | | | F-ICP-AES | | | | | | |
| 62245 | JLO-30-303-2 | 430165 | 6459334 | MPTv | Alkali olivine basalt | 48.15 | 15.22 | 10.26 | 0.161 | 6.37 | 7.97 | 3.42 | 1.91 | 1.726 | 0.87 | 1.61 | 97.65 |
| 62266 | LDI-9-73 | 406431 | 6473405 | MPTv | Alkali olivine basalt | 45.42 | 14.95 | 9.87 | 0.167 | 5.75 | 9.45 | 3.53 | 2.97 | 2.095 | 0.82 | 5.43 | 100.5 |
| 62256 | JLO-12-117 | 419804 | 6481015 | PaSPgd | Hb-bt qtz granodiorite | 63.93 | 15.68 | 4.8 | 0.092 | 1.54 | 3.9 | 3.72 | 3.35 | 0.502 | 0.29 | 0.62 | 98.42 |
| 62256 Dup | JLO-12-117 | 419804 | 6481015 | PaSPgd | Hb-bt qtz granodiorite | - | - | - | - | - | - | - | - | - | - | - | - |
| 622456 Orig | JLO-12-117 | 419804 | 6481015 | PaSPgd | Hb-bt qtz granodiorite | - | - | - | - | - | - | - | - | - | - | - | - |
| Difference[3] | JLO-12-117 | 419804 | 6481015 | PaSPgd | Hb-bt qtz granodiorite | - | - | - | - | - | - | - | - | - | - | - | - |
| 62262 | TMC-2-15 | 427037 | 6460554 | MJPm | Hb-bt qtz monzodiorite | 53.55 | 17.78 | 8.89 | 0.155 | 3.77 | 7.68 | 3.74 | 2.77 | 0.987 | 0.31 | 0.28 | 99.9 |
| 62252 | TMC-2-16 | 427372 | 6460293 | MJPm | Hb-bt qtz monzonite | 65.9 | 16.39 | 3.94 | 0.067 | 1.27 | 3.34 | 3.88 | 4.07 | 0.402 | 0.15 | 0.83 | 100.2 |
| 62241 | OIV-3-41 | 428976 | 6454429 | MJPm | Bt-hb monzonite dike | 56.54 | 17.44 | 7.91 | 0.068 | 3.06 | 5.78 | 4.02 | 3.4 | 0.763 | 0.28 | 1.57 | 100.8 |
| 62244 | JLO-21-208 | 441811 | 6450829 | MJPm | Hb-bt quartz monzonite | 72.47 | 14.59 | 1.9 | 0.113 | 0.32 | 1.24 | 4.34 | 4.46 | 0.219 | 0.06 | 0.36 | 100.1 |
| 62271 | LDI-19-165 | 425101 | 6458048 | MJPm | Hb-bt qtz monzonite | 64.04 | 16.77 | 4.54 | 0.103 | 1.5 | 3.99 | 3.89 | 3.63 | 0.467 | 0.18 | 0.82 | 99.92 |
| 62272 | LDI-19-165dup | 425101 | 6458048 | MJPm | Hb-bt qtz monzonite | 62.61 | 16.66 | 4.36 | 0.1 | 1.45 | 3.93 | 3.87 | 3.56 | 0.449 | 0.19 | 0.8 | 97.98 |
| Difference[3] | LDI-19-165dif | 425101 | 6458048 | MJPm | Hb-bt qtz monzonite | 0.56 | 0.16 | 1.01 | 0.74 | 0.85 | 0.38 | 0.13 | 0.49 | 0.98 | 1.35 | 0.62 | 0.49 |
| 62249 | DMO-33-288 | 438158 | 6461969 | MJPm | Hb monzodiorite | 55.19 | 16.29 | 8.83 | 0.117 | 3.1 | 5.68 | 3.59 | 4.01 | 0.824 | 0.41 | 1.17 | 99.2 |
| 62257 | DMO-23-182 | 439708 | 6458108 | MJPm? | Hb porphyry | 50.66 | 16.84 | 9.75 | 0.2 | 4.09 | 6.54 | 4.25 | 2.16 | 0.782 | 0.34 | 2.95 | 98.56 |
| 62251 | TMC-7-51 | 427980 | 6467206 | MJHsy | Syenite | 53.08 | 17.47 | 7.71 | 0.184 | 2.22 | 5.4 | 4.31 | 5.57 | 0.667 | 0.35 | 3.39 | 100.4 |
| 62242 | JLO-9-77 | 426788 | 6477834 | LJqfp | Plag porphyry dike | 66.57 | 16.42 | 2.87 | 0.052 | 1.27 | 3.6 | 4.56 | 1.48 | 0.359 | 0.12 | 2.95 | 100.2 |
| 62242 Dup | JLO-9-77 | 426788 | 6477834 | LJqfp | Plag porphyry dike | - | - | - | - | - | - | - | - | - | - | - | - |
| 62242 Orig | JLO-9-77 | 426788 | 6477834 | LJqfp | Plag porphyry dike | - | - | - | - | - | - | - | - | - | - | - | - |
| Difference[3] | JLO-9-77 | 426788 | 6477834 | LJqfp | Plag porphyry dike | - | - | - | - | - | - | - | - | - | - | - | - |
| - | 11OiV4-51A | 455201 | 6457065 | emJHv | augite porphyry | 49.65 | 16.13 | 10.84 | 0.184 | 5.79 | 8.14 | 3.32 | 1.44 | 0.85 | 0.30 | 2.72 | 99.36 |
| - | 11OiV4-51B | 455201 | 6457065 | emJHv | augite porphyry | 48.99 | 16.53 | 10.53 | 0.184 | 5.25 | 8.89 | 2.19 | 2.47 | 0.86 | 0.31 | 2.51 | 98.71 |
| - | 11OiV4-51C | 455201 | 6457065 | emJHv | augite porphyry | 48.72 | 15.94 | 9.92 | 0.175 | 5.18 | 10.65 | 2.24 | 1.98 | 0.8 | 0.29 | 3.19 | 99.09 |
| - | 11OiV4-54 | 454810 | 6457137 | emJHv | augite porphyry | 49.16 | 15.78 | 11.31 | 0.214 | 6.4 | 8.61 | 3.02 | 1.38 | 0.86 | 0.29 | 3.09 | 100.11 |
| - | 11OiV4-55 | 454734 | 6457158 | emJHv | augite porphyry | 47.98 | 16.17 | 11.51 | 0.207 | 5.74 | 9.91 | 1.84 | 1.98 | 0.9 | 0.33 | 3.10 | 99.67 |
| - | 11OiV4-59 | 454470 | 6457278 | emJHv | augite porphyry | 49.68 | 13.34 | 10.11 | 0.187 | 8.93 | 10.63 | 1.83 | 1.26 | 0.76 | 0.15 | 2.46 | 99.34 |
| - | 11OiV4-60 | 454247 | 6457302 | emJHv | augite porphyry | 46.67 | 14.16 | 10.96 | 0.195 | 7.32 | 11.88 | 1.49 | 1.78 | 0.79 | 0.26 | 3.81 | 99.31 |
| - | 11OiV4-61 | 454066 | 6457422 | emJHv | augite porphyry | 47.19 | 14.82 | 11.31 | 0.209 | 7.03 | 11.43 | 2.07 | 1.4 | 0.81 | 0.27 | 3.46 | 99.99 |
| 62258 | DMO-19-154 | 408808 | 6466301 | TJgb | Hb diorite | 47.84 | 19.3 | 10.44 | 0.22 | 3.94 | 11.03 | 3.59 | 1.2 | 0.902 | 0.56 | 1.82 | 100.8 |
| 62248 | JLO-22-215 | 419963 | 6460563 | TJgb | Hb gabbro, diorite | 45.81 | 15.21 | 11.88 | 0.193 | 8.38 | 12.01 | 2.22 | 1.35 | 1.069 | 0.25 | 1.94 | 100.3 |
| 62248 Dup | JLO-22-215 | 419963 | 6460563 | TJgb | Hb gabbro, diorite | 45.96 | 15.33 | 11.91 | 0.193 | 8.33 | 12 | 2.23 | 1.36 | 1.068 | 0.25 | 1.94 | 100.6 |
| 622482 Orig | JLO-22-215 | 419963 | 6460563 | TJgb | Hb gabbro, diorite | 45.67 | 15.1 | 11.85 | 0.193 | 8.43 | 12.02 | 2.22 | 1.35 | 1.071 | 0.25 | 1.94 | 100.1 |
| Difference[3] | JLO-22-215 | 419963 | 6460563 | TJgb | Hb gabbro, diorite | 0.16 | 0.38 | 0.13 | 0 | 0.30 | 0.04 | 0.11 | 0.18 | 0.07 | 0 | 0 | 0.12 |
| 62263 | JLO-20-190 | 455198 | 6456114 | LTCH | Bt-hb qtz monzodiorite | 66.71 | 16.53 | 3.45 | 0.075 | 1.26 | 2.91 | 5.12 | 3.68 | 0.388 | 0.15 | 0.62 | 100.9 |
| 62237 | JLO-14-141-2 | 406973 | 6476844 | lTSpx | Augite-phyric basalt | 45.65 | 11.52 | 11.51 | 0.212 | 8.97 | 11.59 | 1.96 | 2.66 | 0.699 | 0.74 | 4.72 | 100.2 |

**Table 1.** Part I (continued)

| Sample numbers | | Sample location[1] | | | Analyte Symbol: | $SiO_2$ | $Al_2O_3$ | $Fe_2O_3^{(T)}$ | MnO | MgO | CaO | $Na_2O$ | $K_2O$ | $TiO_2$ | $P_2O_5$ | LOI | Total |
|---|---|---|---|---|---|---|---|---|---|---|---|---|---|---|---|---|---|
| | | | | | Unit: | % | % | % | % | % | % | % | % | % | % | % | % |
| | | | | | Detection limit: | 0.01 | 0.01 | 0.01 | 0.001 | 0.01 | 0.01 | 0.01 | 0.01 | 0.001 | 0.01 | | 0.01 |
| Geochemical | Original | Easting | Northing | Unit[5] | Sample description | | | | | | F-ICP-AES | | | | | | |
| 62243 | JLO-16-161-2 | 403267 | 6478913 | lTrSpx | Augite-phyric basalt | 50.34 | 16.8 | 10.41 | 0.16 | 4.7 | 7.8 | 4.21 | 1.74 | 0.946 | 0.31 | 2.95 | 100.4 |
| 62259 | JLO-16-153 | 405565 | 6479260 | lTrSpx | Augite-phyric basalt | 49.03 | 14.98 | 11.58 | 0.181 | 5.9 | 7.84 | 2.49 | 3.53 | 0.847 | 0.34 | 2.25 | 98.97 |
| 62260 | JLO-16-153dup | 405565 | 6479260 | lTrSpx | Augite-phyric basalt | 48.51 | 14.64 | 11.45 | 0.182 | 5.96 | 7.94 | 2.47 | 3.44 | 0.838 | 0.34 | 2.3 | 98.08 |
| Difference[3] | JLO-16-153dif | 405565 | 6479260 | lTrSpx | Augite-phyric basalt | 0.27 | 0.57 | 0.28 | 0.14 | 0.25 | 0.32 | 0.20 | 0.65 | 0.27 | 0 | 0.55 | 0.23 |
| 62250 | DMO50-505blank | | | Blank | | 99.89 | 0.06 | 0.4 | 0.004 | 0.01 | 0.02 | 0.02 | < 0.01 | 0.002 | < 0.01 | 0.08 | 100.5 |
| 62247 | DMO-20-158 | 431568 | 6466583 | lTrSmv | Trachyte porphyry | 50.04 | 16.49 | 8.21 | 0.236 | 2.02 | 5.27 | 2.86 | 6.59 | 0.642 | 0.31 | 7.04 | 99.71 |
| 62255 | DMO-33-286 | 429718 | 6466035 | lTrSmv | Latite | 48.78 | 14.43 | 9.27 | 0.2 | 2.98 | 5.09 | 4.64 | 4.63 | 0.722 | 0.33 | 8.32 | 99.39 |
| - | 11JLO21-203 | 442981 | 6452092 | lTrSmv | Plag-phyric basalt | 51.75 | 17.59 | 9.06 | 0.063 | 2.17 | 6.4 | 3.46 | 4.98 | 0.844 | 0.56 | 1.73 | 98.61 |
| 62253 | DMO-29-246 | 417886 | 6464947 | lTrSpp | Plag-phyric basalt | 54.1 | 17.85 | 9.96 | 0.178 | 2.62 | 7.74 | 3.61 | 1.21 | 0.947 | 0.3 | 2.29 | 100.8 |
| 62254 | DMO-30-255 | 406627 | 6466547 | lTrSpp | Plag-phyric basalt | 48.36 | 18.13 | 11.16 | 0.2 | 3.66 | 9.98 | 3.14 | 1.34 | 1.062 | 0.26 | 1.95 | 99.23 |
| 62239 | DMO-18-138 | 406068 | 6479589 | lTrSpp | Plag-phyric basalt | 52.09 | 17.78 | 9.77 | 0.271 | 3.16 | 3.87 | 2.79 | 6.74 | 0.778 | 0.74 | 2.97 | 101 |
| 62261 | JLO-17-172 | 413803 | 6470151 | lTrSpp | Plag-phyric basalt | 60.53 | 17.7 | 5.2 | 0.188 | 1.33 | 3.42 | 6.7 | 3.11 | 0.81 | 0.39 | 1.61 | 101 |
| 62268 | LDI-12-96 | 405326 | 6479731 | lTrSpp | Plag-phyric basalt | 53.55 | 18.45 | 7.02 | 0.274 | 2.39 | 1.67 | 0.9 | 11.15 | 0.822 | 0.35 | 2.19 | 98.77 |
| 62269 | LDI-12-97 | 405246 | 6479876 | lTrSpp | Plag-phyric basalt | 62.07 | 16.68 | 5.01 | 0.206 | 0.76 | 1.5 | 6.92 | 4.29 | 0.804 | 0.3 | 0.72 | 99.25 |
| 62269 Orig | LDI-12-97 | 405246 | 6479876 | lTrSpp | Plag-phyric basalt | - | - | - | - | - | - | - | - | - | - | - | - |
| 62269 Dup | LDI-12-97 | 405246 | 6479876 | lTrSpp | Plag-phyric basalt | - | - | - | - | - | - | - | - | - | - | - | - |
| Difference[3] | LDI-12-97 | 405246 | 6479876 | lTrSpp | Plag-phyric basalt | - | - | - | - | - | - | - | - | - | - | - | - |
| 62273 | DMO-38-337 | 419651 | 6466174 | lTrSpp | Plag-phyric basalt | 50.13 | 16.81 | 11.88 | 0.159 | 4.05 | 8.62 | 2.46 | 1.75 | 0.879 | 0.25 | 2.2 | 99.19 |
| 62240 | JLO-5-42 | 435063 | 6474098 | lTrSv | Aphanitic basalt | 46.99 | 16.92 | 10.8 | 0.144 | 5.23 | 12.55 | 3.05 | 0.02 | 0.826 | 0.19 | 4.16 | 100.9 |
| 62246 | DMO-3-23 | 429719 | 6473685 | lTrSv | Aphyric basalt | 45.54 | 13.46 | 12.1 | 0.248 | 6.41 | 10.31 | 3.24 | 1.72 | 0.821 | 0.11 | 5.54 | 99.5 |
| 62264 | JLO-16-162 | 403037 | 6478945 | lTrSv | Plag crystal tuff | 52.19 | 17.76 | 8.51 | 0.173 | 3.73 | 7.19 | 2.78 | 1.84 | 0.843 | 0.32 | 2.77 | 98.12 |
| 62267 | LDI-12-95 | 405578 | 6479353 | lTrSv | Aphanitic basalt | 50.96 | 15.34 | 10.4 | 0.164 | 5.42 | 7.92 | 4.61 | 1.16 | 0.83 | 0.31 | 2.26 | 99.36 |
| 62270 | LDI-16-137 | 424170 | 6457044 | mTrTv | Augite phyric basalt | 47.68 | 14.2 | 11.36 | 0.188 | 7.46 | 10.84 | 2 | 3.12 | 1.045 | 0.54 | 1.09 | 99.53 |
| 62238 | JLO-23-227 | 416358 | 6462047 | mTrTv | Plag-augite porhyry | 42.34 | 13.36 | 10.51 | 0.32 | 5.26 | 16.53 | 3.2 | 0.56 | 0.847 | 0.23 | 7.81 | 101 |
| - | 11OiV1-2 | 450904 | 6425990 | mTrTv | augite porphyry | 48.41 | 13.01 | 10.99 | 0.208 | 9.52 | 10.88 | 1.1 | 1.58 | 0.82 | 0.44 | 1.94 | 98.90 |
| - | 11LDi18-145B | 442227 | 6447684 | mTrTv | augite porphyry | 49.91 | 12.01 | 10.34 | 0.17 | 8.92 | 9.55 | 0.56 | 3.72 | 0.54 | 0.54 | 0.00 | 96.26 |
| - | 11LDi18-147 | 442601 | 6447993 | mTrTv | augite porphyry | 50.95 | 16.73 | 10.14 | 0.187 | 6.08 | 6.46 | 3.86 | 2.03 | 0.7 | 0.24 | 0.77 | 98.15 |
| - | 11LDi18-151 | 443194 | 6448373 | mTrTv | augite porphyry | 48.97 | 13.22 | 9.79 | 0.164 | 8.99 | 10.62 | 1.46 | 3.19 | 0.69 | 0.64 | 1.10 | 98.83 |
| - | 11LDi18-152 | 443642 | 6448548 | mTrTv | augite porphyry | 49.04 | 13.47 | 9.79 | 0.15 | 8.34 | 11.59 | 1.73 | 2.93 | 0.64 | 0.52 | 0.98 | 99.18 |
| - | 11OiV3-39 | 428941 | 6454305 | mTrTv | augite porphyry | 45.91 | 14.81 | 12.36 | 0.178 | 5.45 | 13.9 | 1.73 | 1.4 | 0.82 | 0.27 | 1.56 | 98.39 |
| - | 11OiV5-72 | 441164 | 6450773 | mTrTv | augite porphyry | 45.84 | 14.25 | 11.84 | 0.306 | 7.37 | 15.14 | 0.74 | 1.67 | 0.54 | 0.39 | 0.42 | 98.50 |
| - | 11OiV5-73 | 441106 | 6450910 | mTrTv | augite porphyry | 47.91 | 13.33 | 11.55 | 0.195 | 8.16 | 10.12 | 1.79 | 3.07 | 0.69 | 0.57 | 0.83 | 98.21 |
| - | 11OiV5-74 | 441143 | 6451142 | mTrTv | augite porphyry | 48.3 | 13.36 | 10.73 | 0.236 | 8.24 | 11.25 | 1.64 | 2.56 | 0.75 | 0.61 | 0.78 | 98.45 |
| - | 11OiV5-75 | 441154 | 6451175 | mTrTv | augite porphyry | 50.23 | 13.86 | 9.09 | 0.212 | 7.82 | 10.68 | 2.63 | 2.11 | 0.74 | 0.63 | 0.85 | 98.84 |
| - | 11JLO21-211-2 | 441542 | 6450144 | mTrTv | augite porphyry | 48.79 | 14.19 | 9.7 | 0.172 | 7.26 | 12.42 | 1.54 | 2.84 | 0.63 | 0.44 | 0.51 | 98.49 |

**Table 1.** Part I (continued)

| Sample numbers | | Sample location[1] | | | Analyte Symbol: | $SiO_2$ | $Al_2O_3$ | $Fe_2O_3^{(T)}$ | MnO | MgO | CaO | $Na_2O$ | $K_2O$ | $TiO_2$ | $P_2O_5$ | LOI | Total |
|---|---|---|---|---|---|---|---|---|---|---|---|---|---|---|---|---|---|
| | | | | | Unit: | % | % | % | % | % | % | % | % | % | % | % | % |
| | | | | | Detection limit: | 0.01 | 0.01 | 0.01 | 0.001 | 0.01 | 0.01 | 0.01 | 0.01 | 0.001 | 0.01 | | 0.01 |
| Geochemical | Original | Easting | Northing | Unit[5] | Sample description | F-ICP-AES | | | | | | | | | | | |
| - | 11JLO21-212 | 441537 | 6450031 | mTTv | augite porphyry | 49.04 | 14.46 | 9.7 | 0.16 | 8.04 | 11.85 | 1.9 | 2 | 0.64 | 0.43 | 0.64 | 98.86 |
| 62265 | LDI-4-29 | 425618 | 6480362 | PzTCCv | metabasalt | 49.45 | 14.55 | 13.71 | 0.191 | 6.04 | 7.06 | 4.35 | 0.27 | 2.015 | 0.24 | 2.43 | 100.3 |
| 62265 Orig | LDI-4-29 | 425618 | 6480362 | PzTCCv | metabasalt | 49.44 | 14.48 | 13.7 | 0.19 | 6.05 | 7.02 | 4.39 | 0.27 | 2.012 | 0.24 | 2.43 | 100.2 |
| 62265 Dup | LDI-4-29 | 425618 | 6480362 | PzTCCv | metabasalt | 49.47 | 14.63 | 13.71 | 0.191 | 6.04 | 7.1 | 4.31 | 0.27 | 2.018 | 0.24 | 2.43 | 100.4 |
| Difference[3] | LDI-4-29 | 425618 | 6480362 | PzTCCv | metabasalt | 0.02 | 0.26 | 0.02 | 0.13 | 0.04 | 0.28 | 0.46 | 0 | 0.07 | 0 | 0 | 0.05 |
| 62274 | MRG1standard | - | - | Standard | - | 39.63 | 8.4 | 17.32 | 0.167 | 13.7 | 14.77 | 0.71 | 0.18 | 3.794 | 0.06 | 1.38 | 100.1 |
| Expected[2] | MRG1standard | - | - | Standard | - | 39.12 | 8.47 | 17.94 | 0.17 | 13.6 | 14.7 | 0.74 | 0.18 | 3.77 | 0.08 | 2.23 | 100.95 |
| Difference[3] | MRG1standard | - | - | Standard | - | 0.3 | -0.2 | -0.9 | -0.4 | 0.2 | 0.1 | -1.0 | 0.0 | 0.2 | -7.1 | -11.8 | -0.2 |
| 62275[4] | SY3standard | - | - | Standard | - | 59.54 | 11.57 | 6.5 | 0.321 | 2.61 | 8.09 | 4.03 | 4.33 | 0.147 | 0.55 | 1.19 | 98.87 |
| 62275 Orig | SY3standard | - | - | Standard | - | 59.24 | 11.47 | 6.53 | 0.323 | 2.61 | 8.14 | 3.98 | 4.27 | 0.146 | 0.55 | 1.19 | 98.45 |
| 62275 Dup | SY3standard | - | - | Standard | - | 59.85 | 11.67 | 6.46 | 0.32 | 2.61 | 8.03 | 4.07 | 4.39 | 0.149 | 0.55 | 1.19 | 99.28 |
| Expected[2] | SY3standard | - | - | Standard | - | 59.68 | 11.76 | 6.49 | 0.32 | 2.67 | 8.25 | 4.12 | 4.23 | 0.15 | 0.54 | 1.31 | 99.52 |
| Difference[3] | SY3standard | - | - | Standard | - | -0.2 | -0.6 | 0.2 | 0.2 | -0.6 | -0.3 | -0.9 | 0.2 | -0.7 | 0.5 | -2.4 | -0.3 |
| Difference[3] | SY3standard | - | - | Standard | - | 0.1 | -0.2 | -0.1 | 0.0 | -0.6 | -0.7 | -0.3 | 0.9 | -0.2 | 0.5 | -2.4 | -0.1 |

[1] Sample location in UTM NAD83, Zone 9 V

[2] Recommended values for CANMET standards shaded green, difference between original and duplicate or expected values shaded blue, informational values unshaded (Govindaraju, 1994).

[3] Difference calculated as follows: 0.5*100*{(x1-x2)/(x1+x2)}

[4] Average value of Activation Labs' duplicate analysis of powdered material

[5] Units: MPTv, Miocene-Pliocene Tuya basalt; PaSPgd, Paleocene Snow Peak granodiorite; MJPm, Middle Jurassic Pallen monzonite; MJHsy, Middle Jurassic Hluey syenite; LJqfp, Late Jurassic quartz feldspar porphyry; emJHv, early to middle Jurassic Hazelton basalt, TJgb, Triassic-Jurassic hornblende gabbro; LTCH, Late Triassic Cake Hill pluton; lTSpx, Late Triassic Stuhini pyroxene porphyry; lTSmv, Late Triassic Stuhini latite porphyry; lTSpp, Late Triassic Stuhini plagioclase porphyry; lTSv, Late Triassic Stuhini aphyric basalt; mTTv, Middle Triassic Tsaybahe pyroxene porphyry; PzTCCv, Paleozoic-Triassic Cache Creek basalt

Abbreviations: F-ICP-AES, fusion–inductively coupled plasma–atomic emmission spectrometry; Hb, hornblende; Bt, biotite; Plag, plagioclase; Qtz, quartz; T, total iron

**Table 1.** Part II: Trace and rare earth element analytical results for volcanic and intrusive rocks collected from the area covered by the Dease Lake (104J) and Cry Lake (104I) map sheets, northern British Columbia.

| Analyte symbol: | Be | Sc | V | Cr | Cr | Co | Ni | Ni | Cu | Zn | Ga | Ge | As | Rb | Y | Zr | Nb | Mo | Ag | In | Sn | Sb | Cs |
|---|---|---|---|---|---|---|---|---|---|---|---|---|---|---|---|---|---|---|---|---|---|---|---|
| Unit: | ppm | ppm | ppm | ppm | ppm | ppm | ppm | ppm | ppm | ppm | ppm | ppm | ppm | ppm | ppm | ppm | ppm | ppm | ppm | ppm | ppm | ppm | ppm |
| Detection limit: | 1 | 1 | 5 | 20 | 5 | 1 | 20 | 1 | 10 | 30 | 1 | 0.5 | 5 | 1 | 0.5 | 1 | 0.2 | 2 | 0.5 | 0.1 | 1 | 0.2 | 0.1 |
| Original sample no. | F-ICP-MS | | | | INAA | F-ICP-MS | | TD-ICP | F-ICP-MS | | | | | | | | | | | | | | |
| JLO-30-303-2 | 2 | 22 | 219 | 160 | 162 | 28 | 90 | 88 | 30 | 110 | 18 | 1.2 | < 5 | 26 | 29.5 | 191 | 23.1 | < 2 | 1.6 | < 0.1 | 1 | < 0.2 | 0.7 |
| LDI-9-73 | 2 | 18 | 198 | 130 | 136 | 31 | 100 | 102 | 40 | 100 | 19 | 1.3 | < 5 | 63 | 22.6 | 248 | 91.7 | 3 | 1.7 | < 0.1 | 2 | < 0.2 | 6.5 |
| JLO-12-117 | 2 | 7 | 78 | < 20 | < 5 | 6 | < 20 | 4 | < 10 | < 30 | 18 | 1.3 | < 5 | 101 | 16.2 | 97 | 18.5 | 13 | 0.8 | < 0.1 | < 1 | < 0.2 | 4.6 |
| JLO-12-117dup | - | - | - | - | - | - | - | 4 | - | - | - | - | - | - | - | - | - | - | - | - | - | - | - |
| JLO-12-117orig | - | - | - | - | - | - | - | 4 | - | - | - | - | - | - | - | - | - | - | - | - | - | - | - |
| JLO-12-117dif | - | - | - | - | - | - | - | 0 | - | - | - | - | - | - | - | - | - | - | - | - | - | - | - |
| TMC-2-15 | 2 | 23 | 301 | < 20 | 15 | 22 | < 20 | 13 | 90 | 80 | 19 | 1.3 | < 5 | 56 | 21.7 | 106 | 4.4 | < 2 | 1 | < 0.1 | < 1 | < 0.2 | 1.5 |
| TMC-2-16 | 2 | 7 | 71 | < 20 | 10 | 7 | < 20 | 6 | 130 | < 30 | 16 | 1.5 | < 5 | 108 | 21.1 | 179 | 8 | 2 | 1.2 | < 0.1 | 1 | < 0.2 | 1.6 |
| OIV-3-41 | 1 | 17 | 203 | < 20 | < 5 | 17 | < 20 | 10 | 100 | < 30 | 17 | 1.3 | < 5 | 65 | 20.6 | 114 | 4.6 | < 2 | 0.8 | < 0.1 | 1 | 0.3 | 0.3 |
| JLO-21-208 | 3 | 2 | 17 | < 20 | 7 | 1 | < 20 | 2 | < 10 | 50 | 16 | 1.8 | < 5 | 100 | 20.9 | 195 | 9.8 | < 2 | 1.4 | < 0.1 | 1 | 0.3 | 1 |
| LDI-19-165 | 2 | 8 | 87 | < 20 | < 5 | 7 | < 20 | 7 | < 10 | 40 | 17 | 0.9 | < 5 | 84 | 24.2 | 204 | 9.5 | < 2 | 1.5 | < 0.1 | 1 | < 0.2 | 1.4 |
| LDI-19-165dup | 2 | 8 | 80 | < 20 | 12 | 7 | < 20 | 7 | < 10 | 40 | 17 | 1.4 | < 5 | 86 | 24.4 | 216 | 9.3 | < 2 | 1.2 | < 0.1 | 2 | < 0.2 | 1.5 |
| LDI-19-165dif | 0 | 0 | 2.10 | 0 | | 0 | 0 | 0 | 0 | 0 | 0 | 10.87 | 0 | 0.59 | 0.21 | 1.43 | 0.53 | 0 | 5.56 | 0 | 16.67 | 0 | 1.72 |
| DMO-33-288 | 3 | 19 | 188 | < 20 | 17 | 20 | < 20 | 12 | 80 | 40 | 18 | 1.3 | < 5 | 122 | 28.4 | 297 | 13.7 | < 2 | 2 | < 0.1 | 2 | 1.1 | 1.2 |
| DMO-23-182 | < 1 | 22 | 252 | 30 | 38 | 21 | < 20 | 16 | 60 | 60 | 18 | 1.6 | < 5 | 36 | 15.8 | 52 | 1.9 | < 2 | 0.5 | < 0.1 | < 1 | 0.8 | 0.2 |
| TMC-7-51 | 4 | 13 | 198 | < 20 | 9 | 16 | < 20 | 8 | 20 | 70 | 18 | 1.3 | < 5 | 162 | 24.9 | 261 | 13.3 | 3 | 2.2 | < 0.1 | 1 | 1.9 | 2.1 |
| JLO-9-77 | < 1 | 6 | 57 | < 20 | 14 | 6 | < 20 | 10 | 30 | 40 | 19 | 0.7 | < 5 | 25 | 6.4 | 67 | 1.3 | < 2 | 0.6 | < 0.1 | < 1 | 1 | 0.6 |
| JLO-9-77dup | - | - | - | - | - | - | - | 10 | - | - | - | - | - | - | - | - | - | - | - | - | - | - | - |
| JLO-9-77orig | - | - | - | - | - | - | - | 10 | - | - | - | - | - | - | - | - | - | - | - | - | - | - | - |
| JLO-9-77dif | - | - | - | - | - | - | - | 0 | - | - | - | - | - | - | - | - | - | - | - | - | - | - | - |
| 11OiV4-51A | - | 29 | 283 | 212 | | 44 | 29 | - | 169 | 75 | 17 | 1.9 | < 5 | 25 | 15.4 | 60 | 1.5 | < 2 | < 0.5 | < 0.1 | < 1 | < 0.2 | 0.9 |
| 11OiV4-51B | - | 26 | 275 | 149 | | 38 | 21 | - | 166 | 79 | 18 | 1.8 | < 5 | 34 | 16.7 | 62 | 1.5 | < 2 | < 0.5 | < 0.1 | < 1 | < 0.2 | 0.8 |
| 11OiV4-51C | - | 27 | 257 | 175 | | 37 | 28 | - | 189 | 69 | 19 | 2.4 | < 5 | 25 | 16.3 | 64 | 1.7 | < 2 | < 0.5 | < 0.1 | < 1 | < 0.2 | < 0.1 |
| 11OiV4-54 | - | 31 | 290 | 215 | | 40 | 37 | - | 147 | 63 | 17 | 1.9 | < 5 | 20 | 15.2 | 57 | 1.3 | < 2 | < 0.5 | < 0.1 | < 1 | < 0.2 | 0.2 |
| 11OiV4-55 | - | 28 | 303 | 154 | | 41 | 25 | - | 173 | 79 | 19 | 2.2 | < 5 | 24 | 16.4 | 50 | 1.1 | < 2 | < 0.5 | < 0.1 | < 1 | < 0.2 | 2.1 |
| 11OiV4-59 | - | 37 | 240 | 264 | | 42 | 58 | - | 105 | 72 | 15 | 2.2 | < 5 | 20 | 17.2 | 63 | 1.1 | < 2 | < 0.5 | < 0.1 | < 1 | < 0.2 | 1 |
| 11OiV4-60 | - | 41 | 277 | 201 | | 44 | 36 | - | 126 | 72 | 17 | 2.5 | < 5 | 24 | 14.6 | 41 | 0.4 | < 2 | < 0.5 | < 0.1 | < 1 | < 0.2 | < 0.1 |
| 11OiV4-61 | - | 39 | 295 | 209 | | 46 | 37 | - | 128 | 65 | 17 | 2.1 | < 5 | 19 | 14.6 | 41 | 0.5 | < 2 | < 0.5 | < 0.1 | < 1 | < 0.2 | 0.3 |
| DMO-19-154 | < 1 | 19 | 289 | < 20 | 14 | 21 | < 20 | 8 | 190 | 110 | 22 | 1.5 | < 5 | 21 | 23.2 | 20 | 1.7 | < 2 | < 0.5 | < 0.1 | < 1 | < 0.2 | 0.6 |
| JLO-22-215 | < 1 | 50 | 428 | 180 | 169 | 37 | 70 | 67 | 60 | 70 | 17 | 1.6 | < 5 | 22 | 16 | 28 | 1.2 | < 2 | < 0.5 | < 0.1 | < 1 | < 0.2 | 0.4 |
| JLO-22-215dup | < 1 | 50 | 429 | 170 | | 37 | 70 | | 60 | 70 | 17 | 1.8 | < 5 | 22 | 16.2 | 28 | 1.2 | < 2 | < 0.5 | < 0.1 | < 1 | < 0.2 | 0.4 |
| JLO-22-215orig | < 1 | 50 | 427 | 180 | | 37 | 70 | | 60 | 70 | 17 | 1.4 | < 5 | 21 | 15.8 | 27 | 1.2 | < 2 | < 0.5 | < 0.1 | < 1 | < 0.2 | 0.4 |
| JLO-22-215dif | 0 | 0 | 0.12 | 1.43 | | 0 | 0 | | 0 | 0 | 0 | 6.25 | 0 | 1.16 | 0.62 | 0.91 | 0 | 0 | 0 | 0 | 0 | 0 | 0 |
| JLO-20-190 | 2 | 5 | 69 | < 20 | 18 | 5 | < 20 | 7 | < 10 | 40 | 20 | 1.5 | < 5 | 84 | 11.9 | 134 | 5.3 | < 2 | 1.3 | < 0.1 | < 1 | 0.3 | 1.1 |
| JLO-14-141-2 | 2 | 38 | 322 | 290 | 297 | 36 | 70 | 69 | 160 | 90 | 13 | 2.5 | < 5 | 47 | 14 | 43 | 3.2 | < 2 | < 0.5 | < 0.1 | < 1 | 0.4 | 0.5 |

**Table 1.** Part II (continued)

| Analyte symbol: | Be | Sc | V | Cr | Cr | Co | Ni | Ni | Cu | Zn | Ga | Ge | As | Rb | Y | Zr | Nb | Mo | Ag | In | Sn | Sb | Cs |
|---|---|---|---|---|---|---|---|---|---|---|---|---|---|---|---|---|---|---|---|---|---|---|---|
| Unit: | ppm | ppm | ppm | ppm | ppm | ppm | ppm | ppm | ppm | ppm | ppm | ppm | ppm | ppm | ppm | ppm | ppm | ppm | ppm | ppm | ppm | ppm | ppm |
| Detection limit: | 1 | 1 | 5 | 20 | 5 | 1 | 20 | 1 | 10 | 30 | 1 | 0.5 | 5 | 1 | 0.5 | 1 | 0.2 | 2 | 0.5 | 0.1 | 1 | 0.2 | 0.1 |
| Original sample no. | F-ICP-MS | | | | INAA | F-ICP-MS | | TD-ICP | F-ICP-MS | | | | | | | | | | | | | | |
| JLO-16-161-2 | < 1 | 29 | 294 | 40 | 44 | 26 | 20 | 26 | 60 | 100 | 18 | 1.8 | < 5 | 37 | 19.9 | 72 | 1.9 | < 2 | < 0.5 | < 0.1 | < 1 | 0.4 | 0.7 |
| JLO-16-153 | < 1 | 32 | 312 | 70 | 79 | 29 | 30 | 21 | 120 | 80 | 17 | 1.3 | < 5 | 73 | 18.9 | 56 | 1.3 | < 2 | < 0.5 | < 0.1 | < 1 | < 0.2 | 1.2 |
| JLO-16-153dup | < 1 | 33 | 313 | 70 | 76 | 30 | 30 | 24 | 120 | 90 | 18 | 1.7 | < 5 | 76 | 19.6 | 57 | 1.3 | < 2 | < 0.5 | < 0.1 | < 1 | < 0.2 | 1.3 |
| JLO-16-153dif | 0 | 0.77 | 0.08 | 0 | 0.97 | 0.85 | 0 | 3.33 | 0 | 2.94 | 1.43 | 6.67 | 0 | 1.01 | 0.91 | 0.44 | 0 | 0 | 0 | 0 | 0 | 0 | 2 |
| DMO50-505blank | < 1 | < 1 | < 5 | < 20 | 11 | < 1 | < 20 | < 1 | < 10 | < 30 | < 1 | 1.5 | < 5 | < 1 | < 0.5 | < 1 | < 0.2 | < 2 | < 0.5 | < 0.1 | < 1 | < 0.2 | < 0.1 |
| DMO-20-158 | 3 | 13 | 191 | < 20 | < 5 | 17 | < 20 | 8 | 10 | 130 | 18 | 1.1 | 7 | 165 | 24.1 | 233 | 11.8 | < 2 | 1.8 | < 0.1 | 2 | 2.9 | 8.1 |
| DMO-33-286 | 1 | 19 | 113 | < 20 | 24 | 16 | < 20 | 10 | 150 | 160 | 13 | 0.9 | 33 | 86 | 21.2 | 182 | 8.8 | < 2 | 1.3 | < 0.1 | < 1 | 1.8 | 0.3 |
| 11JLO21-203 | 2 | 17 | 248 | 40 | | 23 | < 20 | - | 70 | 40 | 20 | 2.2 | 25 | 92 | 24.9 | 177 | 11.4 | < 2 | 1.8 | < 0.1 | < 1 | 3.3 | 2 |
| DMO-29-246 | < 1 | 28 | 285 | < 20 | 12 | 18 | < 20 | 5 | 180 | 100 | 19 | 1.3 | < 5 | 24 | 21.4 | 51 | 1.3 | < 2 | < 0.5 | < 0.1 | < 1 | 0.4 | 1.8 |
| DMO-30-255 | < 1 | 31 | 380 | 30 | 40 | 23 | 20 | 18 | 200 | 90 | 18 | 1.8 | < 5 | 20 | 19.4 | 50 | 1.3 | < 2 | < 0.5 | < 0.1 | < 1 | 0.4 | 0.2 |
| DMO-18-138 | 2 | 8 | 157 | < 20 | 8 | 18 | < 20 | 7 | 230 | 160 | 17 | 1 | < 5 | 101 | 24.8 | 85 | 4.2 | < 2 | 0.7 | < 0.1 | < 1 | 0.3 | 1 |
| JLO-17-172 | 2 | 6 | 140 | < 20 | 8 | 7 | < 20 | 3 | 40 | 150 | 22 | 1.7 | < 5 | 32 | 26.8 | 123 | 6.7 | < 2 | 1 | < 0.1 | 1 | 1.1 | 0.6 |
| LDI-12-96 | 2 | 6 | 160 | < 20 | < 5 | 8 | < 20 | 4 | 200 | 130 | 18 | 1.4 | < 5 | 235 | 24.1 | 111 | 4.4 | < 2 | 0.8 | < 0.1 | 1 | 1 | 10.6 |
| LDI-12-97 | 2 | 5 | 139 | < 20 | < 5 | 4 | < 20 | 3 | 20 | 160 | 17 | 1.1 | < 5 | 49 | 21.5 | 85 | 3.5 | < 2 | 0.5 | < 0.1 | 1 | 0.5 | 2.7 |
| LDI-12-97orig | - | - | - | - | - | - | - | 3 | - | - | - | - | - | - | - | - | - | - | - | - | - | - | - |
| LDI-12-97dup | - | - | - | - | - | - | - | 3 | - | - | - | - | - | - | - | - | - | - | - | - | - | - | - |
| LDI-12-97dif | - | - | - | - | - | - | - | 0 | - | - | - | - | - | - | - | - | - | - | - | - | - | - | - |
| DMO-38-337 | < 1 | 30 | 346 | 40 | 43 | 29 | 20 | 25 | 180 | 90 | 18 | 1.3 | < 5 | 36 | 18.2 | 51 | 1.6 | < 2 | < 0.5 | < 0.1 | < 1 | 0.4 | 1 |
| JLO-5-42 | < 1 | 32 | 344 | 60 | 61 | 31 | 30 | 25 | 120 | 70 | 21 | 2.1 | < 5 | < 1 | 15.6 | 48 | 1.5 | < 2 | < 0.5 | < 0.1 | < 1 | < 0.2 | 0.5 |
| DMO-3-23 | < 1 | 55 | 382 | 220 | 234 | 42 | 50 | 59 | 100 | 80 | 13 | 0.7 | < 5 | 32 | 14.7 | 33 | 1 | 3 | < 0.5 | < 0.1 | < 1 | < 0.2 | 0.7 |
| JLO-16-162 | 1 | 20 | 207 | < 20 | 12 | 16 | < 20 | 8 | 50 | 90 | 19 | 1.2 | < 5 | 58 | 22.2 | 100 | 2.7 | < 2 | 0.7 | < 0.1 | < 1 | 0.3 | 0.8 |
| LDI-12-95 | < 1 | 29 | 287 | 50 | 56 | 27 | 20 | 19 | 110 | 90 | 15 | 1.6 | < 5 | 18 | 19 | 60 | 2 | < 2 | < 0.5 | < 0.1 | < 1 | < 0.2 | 0.8 |
| LDI-16-137 | 2 | 42 | 349 | 150 | 155 | 33 | 60 | 64 | 120 | 100 | 16 | 2 | < 5 | 51 | 19.7 | 72 | 2.3 | < 2 | 0.6 | < 0.1 | < 1 | < 0.2 | 0.5 |
| JLO-23-227 | < 1 | 38 | 373 | 30 | 22 | 26 | 20 | 16 | 130 | 70 | 14 | 1.5 | < 5 | 7 | 15.7 | 33 | 0.7 | < 2 | < 0.5 | < 0.1 | < 1 | 0.3 | 0.1 |
| 11OiV1-2 | - | 46 | 278 | 376 | | 47 | 88 | - | 127 | 66 | 14 | 2 | < 5 | 30 | 15.5 | 47 | 0.4 | < 2 | < 0.5 | < 0.1 | < 1 | < 0.2 | 0.3 |
| 11LDi18-145B | - | 31 | 243 | 506 | | 48 | 94 | - | 193 | 67 | 12 | 2 | < 5 | 43 | 11 | 28 | < 0.2 | < 2 | < 0.5 | < 0.1 | < 1 | < 0.2 | 0.9 |
| 11LDi18-147 | - | 27 | 280 | 279 | | 39 | 82 | - | 210 | 76 | 15 | 1.9 | < 5 | 38 | 13.1 | 36 | 0.4 | < 2 | < 0.5 | < 0.1 | < 1 | 0.4 | 2.4 |
| 11LDi18-151 | - | 35 | 253 | 362 | | 40 | 79 | - | 151 | 73 | 13 | 2.3 | < 5 | 51 | 13.2 | 43 | 0.7 | < 2 | < 0.5 | < 0.1 | < 1 | < 0.2 | 1.6 |
| 11LDi18-152 | - | 37 | 259 | 266 | | 35 | 45 | - | 81 | 63 | 14 | 2.1 | < 5 | 52 | 12.2 | 33 | 0.6 | < 2 | < 0.5 | < 0.1 | < 1 | 0.3 | 0.8 |
| 11OiV3-39 | - | 36 | 288 | 178 | | 40 | 30 | - | 40 | 42 | 16 | 2 | < 5 | 19 | 16.4 | 47 | 0.4 | < 2 | < 0.5 | < 0.1 | < 1 | 0.5 | 0.8 |
| 11OiV5-72 | - | 36 | 223 | 393 | | 44 | 83 | - | 5 | 147 | 14 | 2.3 | < 5 | 24 | 10.8 | 28 | < 0.2 | < 2 | < 0.5 | < 0.1 | 1 | 1.4 | 0.6 |
| 11OiV5-73 | - | 29 | 274 | 283 | | 38 | 75 | - | 12 | 99 | 14 | 2.1 | < 5 | 46 | 14.5 | 43 | 0.3 | < 2 | < 0.5 | < 0.1 | < 1 | 0.5 | 1.1 |
| 11OiV5-74 | - | 38 | 283 | 265 | | 42 | 68 | - | 156 | 93 | 14 | 2.7 | < 5 | 43 | 14.4 | 44 | 0.2 | < 2 | < 0.5 | < 0.1 | < 1 | < 0.2 | 1.2 |
| 11OiV5-75 | - | 31 | 257 | 266 | | 38 | 101 | - | 46 | 124 | 13 | 2.1 | < 5 | 46 | 14 | 45 | 0.3 | < 2 | < 0.5 | < 0.1 | < 1 | < 0.2 | 1.8 |
| 11JLO21-211-2 | - | 33 | 250 | 262 | | 36 | 44 | - | 123 | 49 | 13 | 2.1 | < 5 | 45 | 12.3 | 30 | 0.7 | < 2 | < 0.5 | < 0.1 | < 1 | 0.7 | 0.9 |

**Table 1.** Part II (continued)

| Analyte symbol: | Be | Sc | V | Cr | Cr | Co | Ni | Ni | Cu | Zn | Ga | Ge | As | Rb | Y | Zr | Nb | Mo | Ag | In | Sn | Sb | Cs |
|---|---|---|---|---|---|---|---|---|---|---|---|---|---|---|---|---|---|---|---|---|---|---|---|
| Unit: | ppm | ppm | ppm | ppm | ppm | ppm | ppm | ppm | ppm | ppm | ppm | ppm | ppm | ppm | ppm | ppm | ppm | ppm | ppm | ppm | ppm | ppm | ppm |
| Detection limit: | 1 | 1 | 5 | 20 | 5 | 1 | 20 | 1 | 10 | 30 | 1 | 0.5 | 5 | 1 | 0.5 | 1 | 0.2 | 2 | 0.5 | 0.1 | 1 | 0.2 | 0.1 |
| Original sample no. | F-ICP-MS | | | | INAA | F-ICP-MS | | TD-ICP | F-ICP-MS | | | | | | | | | | | | | | |
| 11JLO21-212 | - | 40 | 263 | 294 | | 39 | 55 | - | 168 | 49 | 15 | 2.4 | < 5 | 38 | 13.2 | 36 | 0.8 | < 2 | < 0.5 | < 0.1 | < 1 | 0.3 | 0.7 |
| LDI-4-29 | < 1 | 45 | 422 | 30 | 37 | 40 | 40 | 41 | 500 | 140 | 18 | 1.8 | < 5 | 4 | 31.6 | 134 | 8.6 | < 2 | 0.9 | < 0.1 | < 1 | < 0.2 | 0.7 |
| LDI-4-29orig | < 1 | 45 | 422 | 30 | | 39 | 40 | | 500 | 140 | 18 | 1.8 | < 5 | 4 | 31.4 | 133 | 8.5 | < 2 | 0.9 | < 0.1 | < 1 | 0.5 | 0.7 |
| LDI-4-29dup | < 1 | 45 | 423 | 30 | | 40 | 40 | | 500 | 140 | 18 | 1.9 | < 5 | 4 | 31.7 | 135 | 8.8 | < 2 | 1 | < 0.1 | < 1 | < 0.2 | 0.8 |
| LDI-4-29dif | 0 | 0 | 0.06 | 0 | | 0.63 | 0 | | 0 | 0 | 0 | 1.35 | 0 | 0 | 0.24 | 0.37 | 0.87 | 0 | 2.63 | 0 | 0 | 0 | 3.33 |
| MRG1standard | <1 | 54 | 541 | 430 | 440 | 79 | 170 | 179 | 130 | 220 | 19 | 1.4 | <5 | 7 | 12.1 | 99 | 18.1 | <2 | 1.2 | <0.1 | 6 | 0.7 | 0.6 |
| MRG1expected | 0.61 | 55 | 526 | 430 | 430 | 87 | 193 | 193 | 134 | 191 | 17 | | 0.73 | 8.5 | 14 | 108 | 20 | 0.87 | 0.11 | | 3.6 | 0.86 | 0.57 |
| MRG1dif | | -0.5 | 0.7 | 0.0 | 0.6 | -2.4 | -3.2 | -1.9 | -0.8 | 3.5 | 2.8 | | | -4.8 | -3.6 | -2.2 | -2.5 | | 41.6 | | 12.5 | -5.1 | 1.3 |
| SY3standard | 24 | 8 | 55 | <20 | 54 | 7 | <20 | 7 | 20 | 250 | 33 | 2.4 | 18 | 197 | 675 | 351 | 182 | <2 | 2.4 | <0.1 | 7 | 3.3 | 2.6 |
| SY3orig | 24 | 8 | 55 | <20 | | 7 | <20 | | 20 | 250 | 33 | 2.2 | 18 | 195 | 675 | 357 | 183 | <2 | 2.3 | <0.1 | 8 | 0.2 | 2.6 |
| SY3dup | 24 | 8 | 55 | <20 | | 8 | <20 | | 10 | 250 | 32 | 2.6 | 19 | 198 | 674 | 345 | 180 | <2 | 2.4 | <0.1 | 7 | 6.4 | 2.7 |
| SY3expected | 20 | 6.8 | 50 | 11 | 11 | 8.8 | 11 | 11 | 17 | 244 | 27 | 1.4 | 18.8 | 206 | 718 | 320 | 148 | 1 | 1.5 | | 6.5 | 0.31 | 2.5 |
| SY3dif | 4.5 | 4.1 | 2.4 | | | -5.7 | | | 4.1 | 0.6 | 5.0 | 11.1 | -1.1 | -1.4 | -1.5 | 2.7 | 5.3 | | 10.5 | | 5.2 | -10.8 | 1.0 |
| SY3dif | 4.5 | 4.1 | 2.4 | | | -2.4 | | | -13.0 | 0.6 | 4.2 | 15.0 | 0.3 | -1.0 | -1.6 | 1.9 | 4.9 | | 11.5 | | 1.9 | 45.4 | 1.9 |

Abbreviations: F-ICP-MS, fusion–inductively coupled plasma–mass spectrometry; INAA, instrumental neutron activation analysis; TD-ICP, total digestion–inductively coupled plasma–mass spectrometry

Recommended values for CANMET standards shaded green, difference between original and duplicate or expected values shaded blue, informational values unshaded (Govindaraju, 1994).

**Table 1.** Part III: Trace and rare earth element analytical results for volcanic and intrusive rocks collected from the area covered by the Dease Lake (104J) and Cry Lake (104I) map sheets, northern British Columbia.

| Analyte: | La | Ce | Pr | Nd | Sm | Eu | Gd | Tb | Dy | Ho | Er | Tm | Yb | Lu | Hf | Ta | W | Tl | Pb | Bi | Th | U | Sr | Ba |
|---|---|---|---|---|---|---|---|---|---|---|---|---|---|---|---|---|---|---|---|---|---|---|---|---|
| Unit: | ppm | ppm | ppm | ppm | ppm | ppm | ppm | ppm | ppm | ppm | ppm | ppm | ppm | ppm | ppm | ppm | ppm | ppm | ppm | ppm | ppm | ppm | ppm | ppm |
| Detection limit: | 0.05 | 0.05 | 0.01 | 0.05 | 0.01 | 0.005 | 0.01 | 0.01 | 0.01 | 0.01 | 0.01 | 0.005 | 0.01 | 0.002 | 0.1 | 0.01 | 0.5 | 0.05 | 5 | 0.1 | 0.05 | 0.01 | 2 | 3 |
| **Original sample no.** | | | | | | | | | | | | **F-ICP-MS** | | | | | | | | | | | | |
| JLO-30-303-2 | 38.1 | 82.5 | 10.1 | 41.4 | 8.02 | 2.44 | 7.02 | 0.94 | 5.27 | 0.99 | 2.81 | 0.392 | 2.59 | 0.42 | 4 | 1.27 | < 0.5 | 0.17 | 9 | < 0.1 | 3.06 | 1.53 | 1486 | 1250 |
| LDI-9-73 | 53.7 | 102 | 11.2 | 41.4 | 7.55 | 2.39 | 5.47 | 0.86 | 4.4 | 0.82 | 2.14 | 0.303 | 1.94 | 0.31 | 4.8 | 6.74 | < 0.5 | 0.15 | < 5 | < 0.1 | 8.65 | 2.59 | 908 | 1042 |
| JLO-12-117 | 26.4 | 51.5 | 6.01 | 23.6 | 4.51 | 1.18 | 3.29 | 0.54 | 2.72 | 0.52 | 1.48 | 0.222 | 1.61 | 0.29 | 2.5 | 1.66 | 65 | 0.84 | < 5 | < 0.1 | 10.6 | 3.09 | 575 | 953 |
| JLO-12-117dup | - | - | - | - | - | - | - | - | - | - | - | - | - | - | - | - | - | - | - | - | - | - | - | - |
| JLO-12-117orig | - | - | - | - | - | - | - | - | - | - | - | - | - | - | - | - | - | - | - | - | - | - | - | - |
| JLO-12-117dif | - | - | - | - | - | - | - | - | - | - | - | - | - | - | - | - | - | - | - | - | - | - | - | - |
| TMC-2-15 | 19.5 | 40.9 | 5.02 | 21.2 | 4.69 | 1.33 | 4.59 | 0.7 | 3.91 | 0.8 | 2.31 | 0.319 | 1.97 | 0.33 | 2.8 | 0.28 | < 0.5 | 0.21 | 11 | 0.1 | 3.94 | 1.49 | 714 | 974 |
| TMC-2-16 | 27.7 | 50.5 | 5.53 | 21.3 | 4.17 | 0.957 | 3.6 | 0.57 | 3.25 | 0.71 | 2.03 | 0.31 | 2.42 | 0.44 | 4.2 | 0.68 | < 0.5 | 0.41 | 8 | < 0.1 | 14 | 3.15 | 451 | 1091 |
| OIV-3-41 | 20.4 | 39.6 | 4.68 | 18.6 | 4.61 | 1.23 | 3.9 | 0.6 | 3.33 | 0.68 | 1.98 | 0.314 | 2.13 | 0.38 | 2.8 | 0.29 | < 0.5 | 0.15 | < 5 | < 0.1 | 5.26 | 2.26 | 537 | 1220 |
| JLO-21-208 | 35.2 | 63.6 | 6.64 | 24.6 | 4.17 | 0.931 | 3.37 | 0.51 | 3.02 | 0.69 | 2.15 | 0.324 | 2.53 | 0.45 | 4.7 | 0.77 | < 0.5 | 0.37 | 14 | 0.1 | 10.2 | 3.16 | 183 | 1489 |
| LDI-19-165 | 28.6 | 55.8 | 6.35 | 23.9 | 5.12 | 1.21 | 3.99 | 0.66 | 3.75 | 0.77 | 2.53 | 0.392 | 2.49 | 0.47 | 5 | 0.82 | < 0.5 | 0.32 | 9 | < 0.1 | 11.4 | 2.89 | 469 | 1077 |
| LDI-19-165dup | 29.3 | 55.2 | 6.24 | 23.9 | 4.72 | 1.07 | 3.8 | 0.65 | 3.87 | 0.83 | 2.46 | 0.388 | 2.65 | 0.43 | 5.3 | 0.79 | < 0.5 | 0.37 | 10 | < 0.1 | 10.4 | 2.62 | 469 | 1071 |
| LDI-19-165dif | 0.60 | 0.27 | 0.44 | 0 | 2.03 | 3.07 | 1.22 | 0.38 | 0.79 | 1.88 | 0.70 | 0.26 | 1.56 | 2.34 | 1.46 | 0.93 | 0 | 3.62 | 2.63 | 0 | 2.29 | 2.45 | 0 | 0.14 |
| DMO-33-288 | 40.1 | 79.4 | 9.14 | 34.9 | 7.25 | 1.35 | 6.15 | 0.85 | 4.74 | 0.94 | 2.73 | 0.443 | 3.1 | 0.51 | 6.8 | 0.98 | < 0.5 | 0.12 | 5 | < 0.1 | 17.2 | 5.64 | 657 | 971 |
| DMO-23-182 | 12.5 | 26.9 | 3.42 | 16.1 | 3.58 | 1.23 | 3.3 | 0.49 | 2.71 | 0.55 | 1.55 | 0.221 | 1.56 | 0.26 | 1.3 | 0.12 | < 0.5 | 0.33 | < 5 | < 0.1 | 2.67 | 1.63 | 554 | 726 |
| TMC-7-51 | 46.8 | 91.4 | 10.8 | 41 | 7.59 | 1.71 | 5.69 | 0.83 | 4.27 | 0.83 | 2.36 | 0.367 | 2.47 | 0.43 | 5.7 | 0.94 | < 0.5 | 0.23 | 8 | < 0.1 | 22.7 | 9.65 | 1244 | 1450 |
| JLO-9-77 | 5.3 | 12.2 | 1.71 | 7.01 | 1.45 | 0.525 | 1.66 | 0.22 | 1.14 | 0.22 | 0.63 | 0.092 | 0.57 | 0.09 | 1.8 | 0.09 | < 0.5 | 0.16 | < 5 | < 0.1 | 0.64 | 0.44 | 586 | 411 |
| JLO-9-77dup | - | - | - | - | - | - | - | - | - | - | - | - | - | - | - | - | - | - | - | - | - | - | - | - |
| JLO-9-77orig | - | - | - | - | - | - | - | - | - | - | - | - | - | - | - | - | - | - | - | - | - | - | - | - |
| JLO-9-77diff | - | - | - | - | - | - | - | - | - | - | - | - | - | - | - | - | - | - | - | - | - | - | - | - |
| 11OiV4-51A | 15.1 | 31.1 | 3.9 | 17.5 | 4.19 | 1.2 | 3.68 | 0.57 | 3.23 | 0.64 | 1.73 | 0.258 | 1.67 | 0.26 | 1.6 | 0.1 | 25.3 | < 0.05 | < 5 | < 0.1 | 1.98 | 0.82 | 857 | 593 |
| 11OiV4-51B | 16.5 | 33.9 | 4.3 | 19 | 4.35 | 1.38 | 3.8 | 0.61 | 3.38 | 0.65 | 1.81 | 0.275 | 1.86 | 0.3 | 1.7 | 0.05 | 20.5 | 0.05 | 6 | < 0.1 | 1.99 | 0.81 | 823 | 984 |
| 11OiV4-51C | 16.3 | 33 | 4.12 | 17.6 | 3.97 | 1.2 | 3.7 | 0.58 | 3.23 | 0.61 | 1.74 | 0.269 | 1.79 | 0.28 | 1.7 | 0.05 | 18.1 | < 0.05 | 5 | < 0.1 | 2.01 | 0.9 | 399 | 630 |
| 11OiV4-54 | 15.2 | 31.2 | 4.01 | 17.6 | 4.08 | 1.18 | 3.62 | 0.58 | 3.3 | 0.65 | 1.81 | 0.278 | 1.83 | 0.29 | 1.6 | 0.03 | 13.8 | 0.16 | 6 | < 0.1 | 1.92 | 0.77 | 660 | 550 |
| 11OiV4-55 | 15.6 | 31.8 | 4.02 | 18.8 | 4.28 | 1.29 | 3.86 | 0.59 | 3.42 | 0.66 | 1.76 | 0.258 | 1.69 | 0.28 | 1.4 | 0.05 | 12.8 | 0.15 | 6 | < 0.1 | 1.67 | 0.65 | 634 | 915 |
| 11OiV4-59 | 8.88 | 19.5 | 2.6 | 12.2 | 3.18 | 0.94 | 3.15 | 0.55 | 3.4 | 0.68 | 1.94 | 0.294 | 1.96 | 0.32 | 1.6 | 0.03 | 14 | < 0.05 | < 5 | < 0.1 | 1.08 | 0.45 | 414 | 395 |
| 11OiV4-60 | 12.7 | 26.6 | 3.52 | 16 | 4.05 | 1.23 | 3.67 | 0.57 | 3.21 | 0.61 | 1.7 | 0.25 | 1.64 | 0.26 | 1.3 | < 0.01 | 9.9 | < 0.05 | < 5 | < 0.1 | 1.32 | 0.51 | 523 | 747 |
| 11OiV4-61 | 13.2 | 27.2 | 3.54 | 16.2 | 3.87 | 1.31 | 3.58 | 0.53 | 3.14 | 0.6 | 1.72 | 0.244 | 1.58 | 0.25 | 1.2 | < 0.01 | 10.3 | < 0.05 | < 5 | < 0.1 | 1.4 | 0.56 | 574 | 662 |
| DMO-19-154 | 10.9 | 26.8 | 3.8 | 18.9 | 4.77 | 1.53 | 4.97 | 0.68 | 4.1 | 0.82 | 2.37 | 0.315 | 1.95 | 0.32 | 0.8 | 0.04 | < 0.5 | 0.08 | < 5 | < 0.1 | 0.6 | 0.25 | 750 | 370 |
| JLO-22-215 | 6.3 | 15.7 | 2.31 | 11.3 | 3.22 | 1.06 | 3.38 | 0.55 | 2.95 | 0.55 | 1.51 | 0.23 | 1.55 | 0.24 | 1 | 0.06 | < 0.5 | 0.08 | < 5 | < 0.1 | 1.06 | 0.6 | 351 | 244 |
| JLO-22-215dup | 6.32 | 15.9 | 2.33 | 11 | 3.38 | 1.09 | 3.21 | 0.56 | 3.04 | 0.56 | 1.52 | 0.232 | 1.58 | 0.24 | 1 | 0.06 | < 0.5 | 0.08 | < 5 | < 0.1 | 1.08 | 0.65 | 351 | 245 |
| JLO-22-215orig | 6.28 | 15.6 | 2.29 | 11.7 | 3.07 | 1.03 | 3.55 | 0.54 | 2.86 | 0.54 | 1.49 | 0.229 | 1.53 | 0.25 | 1 | 0.05 | < 0.5 | 0.07 | < 5 | < 0.1 | 1.03 | 0.55 | 351 | 244 |
| JLO-22-215dif | 0.16 | 0.48 | 0.43 | 1.54 | 2.40 | 1.42 | 2.51 | 0.91 | 1.53 | 0.91 | 0.50 | 0.33 | 0.80 | 1.14 | 0 | 4.55 | 0 | 3.33 | 0 | 0 | 1.18 | 4.17 | 0 | 0.10 |
| JLO-20-190 | 18 | 34.8 | 4.16 | 16.1 | 2.96 | 0.888 | 2.33 | 0.36 | 1.97 | 0.39 | 1.2 | 0.179 | 1.1 | 0.18 | 3.7 | 0.45 | < 0.5 | 0.3 | 11 | < 0.1 | 5.57 | 1.6 | 921 | 1649 |
| JLO-14-141-2 | 10.7 | 22.6 | 2.88 | 12.1 | 3.05 | 0.91 | 2.76 | 0.46 | 2.56 | 0.51 | 1.41 | 0.193 | 1.29 | 0.22 | 1.3 | 0.14 | < 0.5 | 0.16 | 8 | < 0.1 | 2.69 | 1.02 | 356 | 616 |
| JLO-16-161-2 | 10.8 | 23.8 | 3.13 | 14.2 | 3.72 | 1.18 | 4.11 | 0.62 | 3.33 | 0.69 | 2.05 | 0.309 | 2.08 | 0.35 | 2 | 0.14 | < 0.5 | 0.1 | < 5 | < 0.1 | 1.8 | 0.92 | 414 | 461 |
| JLO-16-153 | 7.88 | 18.2 | 2.58 | 11.3 | 3.48 | 1.08 | 3.67 | 0.6 | 3.49 | 0.7 | 2.01 | 0.307 | 2.15 | 0.35 | 1.7 | 0.06 | < 0.5 | 0.15 | < 5 | < 0.1 | 1.3 | 0.62 | 529 | 1094 |

**Table 1.** Part III (continued)

| Analyte: | La | Ce | Pr | Nd | Sm | Eu | Gd | Tb | Dy | Ho | Er | Tm | Yb | Lu | Hf | Ta | W | Tl | Pb | Bi | Th | U | Sr | Ba |
|---|---|---|---|---|---|---|---|---|---|---|---|---|---|---|---|---|---|---|---|---|---|---|---|---|
| Unit: | ppm | ppm | ppm | ppm | ppm | ppm | ppm | ppm | ppm | ppm | ppm | ppm | ppm | ppm | ppm | ppm | ppm | ppm | ppm | ppm | ppm | ppm | ppm | ppm |
| Detection limit: | 0.05 | 0.05 | 0.01 | 0.05 | 0.01 | 0.005 | 0.01 | 0.01 | 0.01 | 0.01 | 0.01 | 0.005 | 0.01 | 0.002 | 0.1 | 0.01 | 0.5 | 0.05 | 5 | 0.1 | 0.05 | 0.01 | 2 | 3 |
| **Original sample no.** | | | | | | | | | | | | **F-ICP-MS** | | | | | | | | | | | | |
| JLO-16-153 dup | 8.24 | 18.5 | 2.53 | 13.3 | 3.51 | 1.15 | 3.58 | 0.55 | 3.35 | 0.68 | 1.96 | 0.308 | 2.17 | 0.36 | 1.6 | 0.05 | < 0.5 | 0.2 | < 5 | < 0.1 | 1.19 | 0.63 | 524 | 1075 |
| JLO-16-153dif | 1.12 | 0.41 | 0.49 | 4.07 | 0.21 | 1.57 | 0.62 | 2.17 | 1.02 | 0.72 | 0.63 | 0.08 | 0.23 | 0.85 | 1.52 | 4.55 | 0 | 7.14 | 0 | 0 | 2.21 | 0.4 | 0.24 | 0.44 |
| DMO50-505blank | 0.34 | 0.76 | 0.08 | 0.32 | 0.08 | 0.011 | 0.06 | < 0.01 | 0.02 | < 0.01 | < 0.01 | < 0.005 | 0.01 | 0 | < 0.1 | < 0.01 | < 0.5 | < 0.05 | < 5 | < 0.1 | 0.09 | 0.01 | < 2 | 3 |
| DMO-20-158 | 41 | 79.9 | 9.36 | 35.2 | 7.27 | 1.76 | 5.27 | 0.78 | 3.89 | 0.76 | 2.41 | 0.35 | 2.44 | 0.38 | 5.1 | 0.85 | < 0.5 | 0.48 | 8 | < 0.1 | 19.7 | 7.67 | 359 | 1219 |
| DMO-33-286 | 29 | 57.8 | 6.69 | 26.8 | 5.46 | 1.27 | 4.81 | 0.63 | 3.64 | 0.75 | 2.24 | 0.346 | 2.41 | 0.39 | 4.2 | 0.65 | < 0.5 | 0.23 | 9 | < 0.1 | 12.8 | 2.65 | 379 | 924 |
| 11JLO21-203 | 43.1 | 81.6 | 9.68 | 35.9 | 7.3 | 1.63 | 5.61 | 0.85 | 4.83 | 0.89 | 2.52 | 0.37 | 2.58 | 0.43 | 3.8 | 0.85 | 35.6 | 0.11 | 6 | < 0.1 | 11.6 | 4.14 | 1199 | 1652 |
| DMO-29-246 | 8.36 | 19.4 | 2.67 | 13.3 | 3.54 | 1.21 | 3.9 | 0.61 | 3.8 | 0.8 | 2.34 | 0.349 | 2.37 | 0.38 | 1.5 | 0.1 | < 0.5 | 0.06 | < 5 | < 0.1 | 1.34 | 0.76 | 514 | 572 |
| DMO-30-255 | 7.58 | 16.9 | 2.34 | 11.3 | 3.18 | 1.1 | 3.85 | 0.58 | 3.42 | 0.71 | 2.07 | 0.299 | 2.05 | 0.33 | 1.5 | 0.09 | < 0.5 | 0.08 | < 5 | < 0.1 | 1.3 | 0.73 | 279 | 1189 |
| DMO-18-138 | 17.1 | 37.3 | 4.98 | 21.9 | 5.48 | 1.48 | 4.92 | 0.78 | 4.33 | 0.87 | 2.55 | 0.381 | 2.51 | 0.42 | 2.3 | 0.21 | < 0.5 | 0.22 | 10 | < 0.1 | 3.09 | 1.73 | 718 | 2365 |
| JLO-17-172 | 19.9 | 41.8 | 5.3 | 24.8 | 5.71 | 1.55 | 4.71 | 0.83 | 4.32 | 0.93 | 2.78 | 0.423 | 2.8 | 0.45 | 3.3 | 0.49 | < 0.5 | 0.18 | 8 | < 0.1 | 3.21 | 2.03 | 341 | 835 |
| LDI-12-96 | 19.1 | 37.9 | 4.74 | 20.2 | 4.69 | 1.51 | 4.56 | 0.7 | 3.98 | 0.82 | 2.45 | 0.392 | 2.56 | 0.4 | 2.9 | 0.26 | < 0.5 | 0.45 | 15 | < 0.1 | 3.34 | 2.17 | 564 | 3770 |
| LDI-12-97 | 15 | 32.2 | 4.16 | 18.5 | 4.29 | 1.32 | 3.98 | 0.71 | 3.75 | 0.73 | 1.96 | 0.285 | 1.9 | 0.3 | 2.6 | 0.23 | < 0.5 | 0.1 | < 5 | < 0.1 | 2.87 | 0.52 | 151 | 465 |
| LDI-12-97orig | - | - | - | - | - | - | - | - | - | - | - | - | - | - | - | - | - | - | - | - | - | - | - | - |
| LDI-12-97dup | - | - | - | - | - | - | - | - | - | - | - | - | - | - | - | - | - | - | - | - | - | - | - | - |
| LDI-12-97dif | - | - | - | - | - | - | - | - | - | - | - | - | - | - | - | - | - | - | - | - | - | - | - | - |
| DMO-38-337 | 7.68 | 17.5 | 2.39 | 11.5 | 2.87 | 0.997 | 3.14 | 0.52 | 3.19 | 0.68 | 1.97 | 0.293 | 1.9 | 0.3 | 1.5 | 0.09 | < 0.5 | 0.07 | < 5 | < 0.1 | 1.48 | 0.73 | 358 | 650 |
| JLO-5-42 | 10.5 | 22.1 | 2.86 | 13 | 3.1 | 0.916 | 2.93 | 0.5 | 2.77 | 0.56 | 1.58 | 0.229 | 1.44 | 0.23 | 1.5 | 0.11 | < 0.5 | < 0.05 | < 5 | 0.1 | 1.98 | 0.84 | 98 | 20 |
| DMO-3-23 | 6.84 | 15.1 | 2.01 | 9.69 | 2.88 | 0.856 | 2.89 | 0.47 | 2.7 | 0.54 | 1.5 | 0.223 | 1.59 | 0.24 | 1.1 | 0.05 | < 0.5 | 0.33 | < 5 | < 0.1 | 1.24 | 0.48 | 341 | 834 |
| JLO-16-162 | 11.6 | 26.3 | 3.47 | 15.9 | 3.79 | 1.24 | 3.98 | 0.65 | 3.75 | 0.82 | 2.43 | 0.368 | 2.37 | 0.38 | 2.8 | 0.2 | < 0.5 | 0.14 | < 5 | < 0.1 | 2.53 | 1.53 | 529 | 592 |
| LDI-12-95 | 7.72 | 17 | 2.39 | 11.3 | 3.18 | 1.01 | 3.31 | 0.57 | 3.38 | 0.67 | 2 | 0.293 | 1.87 | 0.3 | 1.8 | 0.06 | < 0.5 | 0.06 | < 5 | < 0.1 | 1.2 | 0.58 | 411 | 236 |
| LDI-16-137 | 8.86 | 21.2 | 2.81 | 13.4 | 3.58 | 1.04 | 3.6 | 0.63 | 3.39 | 0.7 | 1.94 | 0.296 | 1.89 | 0.3 | 2 | 0.14 | < 0.5 | 0.11 | < 5 | < 0.1 | 1.42 | 0.73 | 925 | 1378 |
| JLO-23-227 | 3.98 | 9.58 | 1.49 | 7.7 | 2.16 | 0.833 | 2.64 | 0.47 | 2.9 | 0.61 | 1.73 | 0.261 | 1.66 | 0.25 | 1.1 | 0.04 | < 0.5 | < 0.05 | < 5 | < 0.1 | 0.48 | 0.34 | 423 | 243 |
| 11OiV1-2 | 6.13 | 14.8 | 2.22 | 10.2 | 2.98 | 0.953 | 3.3 | 0.53 | 3.2 | 0.65 | 1.86 | 0.276 | 1.73 | 0.26 | 1.4 | 0.03 | 18.6 | < 0.05 | < 5 | < 0.1 | 1.05 | 0.41 | 258 | 369 |
| 11LDi18-145B | 4.65 | 10.4 | 1.48 | 7.22 | 2.05 | 0.699 | 2.42 | 0.4 | 2.34 | 0.47 | 1.34 | 0.204 | 1.37 | 0.22 | 0.9 | < 0.01 | 23.3 | < 0.05 | < 5 | < 0.1 | 0.79 | 0.4 | 453 | 572 |
| 11LDi18-147 | 4.5 | 9.74 | 1.45 | 6.94 | 2.01 | 0.76 | 2.54 | 0.43 | 2.67 | 0.56 | 1.59 | 0.243 | 1.57 | 0.25 | 1.0 | 0.06 | 25.4 | 0.05 | < 5 | < 0.1 | 0.67 | 0.33 | 588 | 716 |
| 11LDi18-151 | 8.41 | 19.6 | 2.59 | 11.4 | 2.8 | 0.868 | 2.74 | 0.46 | 2.75 | 0.52 | 1.44 | 0.219 | 1.45 | 0.23 | 1.2 | 0.01 | 22.2 | 0.05 | < 5 | < 0.1 | 1.61 | 0.62 | 506 | 1013 |
| 11LDi18-152 | 7.89 | 17.6 | 2.33 | 9.78 | 2.4 | 0.762 | 2.55 | 0.43 | 2.54 | 0.52 | 1.5 | 0.213 | 1.37 | 0.22 | 1.0 | 0.05 | 18.1 | < 0.05 | 23 | 0.2 | 1.64 | 0.67 | 349 | 487 |
| 11OiV3-39 | 8.53 | 17.5 | 2.42 | 11.4 | 3.19 | 0.974 | 3.48 | 0.55 | 3.34 | 0.68 | 1.93 | 0.281 | 1.8 | 0.28 | 1.4 | 0.07 | 33.3 | < 0.05 | < 5 | < 0.1 | 0.84 | 0.88 | 352 | 214 |
| 11OiV5-72 | 4.4 | 9.72 | 1.36 | 6.43 | 1.77 | 0.76 | 2.06 | 0.34 | 2.08 | 0.41 | 1.2 | 0.184 | 1.24 | 0.19 | 0.9 | < 0.01 | 22.7 | < 0.05 | 14 | < 0.1 | 0.77 | 1.81 | 365 | 430 |
| 11OiV5-73 | 7.28 | 15.9 | 2.16 | 10.2 | 2.83 | 0.785 | 2.84 | 0.48 | 2.88 | 0.6 | 1.62 | 0.241 | 1.67 | 0.27 | 1.3 | < 0.01 | 10.1 | 0.07 | 7 | < 0.1 | 1.28 | 0.89 | 416 | 539 |
| 11OiV5-74 | 7.62 | 17.6 | 2.49 | 12 | 3.12 | 0.992 | 3.33 | 0.56 | 3.22 | 0.61 | 1.76 | 0.271 | 1.74 | 0.27 | 1.4 | < 0.01 | 21.8 | < 0.05 | 9 | < 0.1 | 1.67 | 0.71 | 504 | 699 |
| 11OiV5-75 | 8.18 | 19 | 2.58 | 12.1 | 3.07 | 0.933 | 3.1 | 0.51 | 2.93 | 0.58 | 1.67 | 0.233 | 1.49 | 0.23 | 1.4 | 0.14 | 20.8 | 0.13 | 7 | < 0.1 | 1.72 | 0.84 | 563 | 544 |
| 11JLO21-211-2 | 4.25 | 9.75 | 1.4 | 6.98 | 2.06 | 0.729 | 2.4 | 0.41 | 2.48 | 0.5 | 1.39 | 0.212 | 1.38 | 0.22 | 0.9 | < 0.01 | 18.9 | < 0.05 | < 5 | < 0.1 | 0.84 | 0.42 | 488 | 597 |
| 11JLO21-212 | 4.56 | 10.8 | 1.58 | 7.59 | 2.11 | 0.777 | 2.44 | 0.43 | 2.73 | 0.55 | 1.56 | 0.228 | 1.44 | 0.23 | 1.1 | 0.02 | 22.5 | < 0.05 | < 5 | < 0.1 | 0.94 | 0.4 | 404 | 447 |
| LDI-4-29 | 8.22 | 22.6 | 3.34 | 16.5 | 4.84 | 1.62 | 5.52 | 0.96 | 5.53 | 1.13 | 3.2 | 0.451 | 3.02 | 0.51 | 3.3 | 0.6 | < 0.5 | < 0.05 | < 5 | < 0.1 | 0.83 | 0.34 | 196 | 49 |
| LDI-4-29orig | 8.41 | 22.7 | 3.29 | 16.1 | 4.8 | 1.67 | 5.42 | 0.95 | 5.53 | 1.13 | 3.16 | 0.446 | 2.97 | 0.52 | 3.1 | 0.59 | < 0.5 | < 0.05 | < 5 | < 0.1 | 0.86 | 0.35 | 196 | 50 |
| LDI-4-29dup | 8.02 | 22.5 | 3.39 | 16.9 | 4.89 | 1.58 | 5.61 | 0.97 | 5.53 | 1.13 | 3.25 | 0.455 | 3.06 | 0.51 | 3.5 | 0.61 | < 0.5 | < 0.05 | < 5 | < 0.1 | 0.8 | 0.33 | 196 | 49 |

**Table 1.** Part III (continued)

| Analyte: | La | Ce | Pr | Nd | Sm | Eu | Gd | Tb | Dy | Ho | Er | Tm | Yb | Lu | Hf | Ta | W | Tl | Pb | Bi | Th | U | Sr | Ba |
|---|---|---|---|---|---|---|---|---|---|---|---|---|---|---|---|---|---|---|---|---|---|---|---|---|
| Unit: | ppm | ppm | ppm | ppm | ppm | ppm | ppm | ppm | ppm | ppm | ppm | ppm | ppm | ppm | ppm | ppm | ppm | ppm | ppm | ppm | ppm | ppm | ppm | ppm |
| Detection limit: | 0.05 | 0.05 | 0.01 | 0.05 | 0.01 | 0.005 | 0.01 | 0.01 | 0.01 | 0.01 | 0.01 | 0.005 | 0.01 | 0.002 | 0.1 | 0.01 | 0.5 | 0.05 | 5 | 0.1 | 0.05 | 0.01 | 2 | 3 |
| **Original sample no.** | | | | | | | | | | | | **F-ICP-MS** | | | | | | | | | | | | |
| LDI-4-29dif | 1.19 | 0.22 | 0.75 | 1.21 | 0.46 | 1.38 | 0.86 | 0.52 | 0 | 0 | 0.70 | 0.50 | 0.75 | 0.54 | 3.03 | 0.83 | 0 | 0 | 0 | 0 | 1.81 | 1.47 | 0 | 0.51 |
| MRG1standard | 9.21 | 25.7 | 3.63 | 17.2 | 4.28 | 1.5 | 4.13 | 0.55 | 2.8 | 0.51 | 1.2 | 0.133 | 0.77 | 0.12 | 3.8 | 0.87 | <0.5 | <0.05 | 9 | 0.2 | 0.83 | 0.3 | 270 | 52 |
| MRG1expected | 9.8 | 26 | 3.4 | 19.2 | 4.5 | 1.39 | 4 | 0.51 | 2.9 | 0.49 | 1.12 | 0.11 | 0.6 | 0.12 | 3.76 | 0.8 | 0.3 | 0.055 | 10 | 0.13 | 0.93 | 0.24 | 266 | 61 |
| MRG1dif | -1.6 | -0.3 | 1.6 | -2.7 | -1.3 | 1.9 | 0.8 | 1.9 | -0.9 | 1.0 | 1.7 | 4.7 | 6.2 | 0.0 | 0.3 | 2.1 | | | -2.6 | 10.6 | -2.8 | 5.6 | 0.4 | -4.0 |
| SY3standard | 1210 | 2150 | 208 | 690 | 119 | 17 | 104 | 19.2 | 117 | 25.5 | 77.7 | 11.3 | 63.9 | 8.51 | 10.2 | 24.7 | <0.5 | 1.31 | 394 | 0.4 | 991 | 667 | 302 | 450 |
| SY3orig | 1210 | 2150 | 208 | 688 | 118 | 17 | 106 | 19.2 | 118 | 24.8 | 77.1 | 11.3 | 63.6 | 8.54 | 9.8 | 24.9 | <0.5 | 1.27 | 372 | 0.3 | 984 | 670 | 301 | 448 |
| SY3dup | 1220 | 2150 | 209 | 691 | 119 | 17 | 102 | 19.3 | 117 | 26.1 | 78.3 | 11.3 | 64.3 | 8.47 | 10.6 | 24.4 | <0.5 | 1.34 | 415 | 0.4 | 999 | 663 | 303 | 452 |
| SY3expected | 1340 | 2230 | 223 | 670 | 109 | 17 | 105 | 18 | 118 | 29.5 | 68 | 11.6 | 62 | 7.9 | 9.7 | 30 | 1.1 | 1.5 | 133 | 0.8 | 1003 | 650 | 302 | 450 |
| SY3dif | -2.5 | -0.9 | -1.7 | 0.7 | 2.0 | 0.0 | 0.2 | 1.6 | 0.0 | -4.3 | 3.1 | -0.7 | 0.6 | 1.9 | 0.3 | -4.6 | | -4.2 | 23.7 | -22.7 | -0.5 | 0.8 | -0.1 | -0.1 |
| SY3dif | -2.3 | -0.9 | -1.6 | 0.8 | 2.2 | 0.0 | -0.7 | 1.7 | -0.2 | -3.1 | 3.5 | -0.7 | 0.9 | 1.7 | 2.2 | -5.1 | | -2.8 | 25.7 | -16.7 | -0.1 | 0.5 | 0.1 | 0.1 |

Abbreviation: F-ICP-MS, fusion-inductively coupled plasma-mass spectrometry

Recommended values for CANMET standards shaded green, difference between original and duplicate or expected values shaded blue, informational values unshaded (Govindaraju, 1994).

were pulverized in a mild steel mill to prevent Cr and Ni contamination and analyzed for major and trace elements using a lithium metaborate plus lithium tetraborate fusion technique. The milled samples were mixed with a flux of lithium metaborate and lithium tetraborate and fused in an induction furnace at 1150°C. The melt was immediately poured into a solution of 5% nitric acid and mixed continuously until completely dissolved. This aggressive fusion technique ensures that the entire sample, including resistate phases, dissolves. The samples were analyzed for major oxides using an inductively coupled plasma–atomic emission spectrometry (ICP-AES) technique and trace elements, including rare earth elements, using an inductively coupled plasma–mass spectrometry (ICP-MS) technique. Nickel was analyzed by an ICP-MS technique following a four acid digestion; beginning with hydrofluoric acid, followed by a mixture of nitric and perchloric acid, and finally hydrochloric acid dissolution. With this near total digestion technique, certain resistate phases (e.g., zircon, monazite, sphene, gahnite, chromite, cassiterite, rutile and barite) may be only partly solubilized. Chromium was analyzed using instrumental neutron activation analysis (INAA), whereby samples were irradiated in a nuclear reactor and, following a 7-day decay, gamma rays measured on germanium detectors. Analytical techniques and detection limits for all major oxides and trace elements are listed in Table 1. Two blind CANMET standards (see Govindaraju, 1994 for reference values) and two blind duplicates of the jaw-crushed material were included in the sample batch. Additional internal quality control duplicate analyses from Activation Labs on powdered samples are also listed in Table 1.

During sample collection every effort was taken to avoid altered material. We removed any obvious surface weathering, veins and amygdules. However, petrography shows that many of the samples are significantly altered, making the use of major elements for classification or discrimination of petrochemical environments suspect. Geochemical results presented in Table 1 show acceptable total weight percent values (between 96.3 and 101 wt. %) and loss on ignition values (between 0.28 and 7.8 wt. %).

## Geochemical Suites Description and Results

### Tsaybahe Group

The Tsaybahe Group comprises mafic volcanic rocks interlayered with Middle Triassic limestone, chert and siliceous thin-bedded sedimentary rocks. It is exposed in the canyon of the Stikine River (Read, 1984) and extends north into the Dease Lake area (Gabrielse, 1998; Logan et al., 2012b, c). The unit is characterized by thick accumulations (200–270 m) of crowded augite-phyric basalt, basalt breccia and volcanic-derived clastic rocks. The basalt contains 1–3 mm, dark green euhedral pyroxene phenocrysts (20–30%) and 0.5–1 mm, stubby white plagioclase laths (5–20%) within an aphanitic, often vesicular or amygdaloidal green- or orange-weathering groundmass (Figure 3a, b, plane-polarized light and crossed nicols). The basalt is deformed and hornfelsed to a biotite-bearing metavolcanic rock adjacent to the Middle Jurassic Pallen Creek pluton (Logan et al., 2012c), but elsewhere it is only weakly altered to lower greenschist mineral assemblages that do not define a penetrative foliation.

Eight samples of flow breccia, two samples of tuff breccia and one sample from a massive flow plot in subalkalic basalt and andesite fields on the Zr/Ti versus Nb/Y classification diagram of Pearce (1996) (Figure 4a). All the samples plot as shoshonite or high-K calcalkaline series on the $SiO_2$ versus $K_2O$ diagram of Peccerillo and Taylor (1976) and in the arc field (Shervais, 1982) and calcalkaline-arc basalt field (Wood, 1980) on tectonic discrimination diagrams (Figure 4b, c, d). Typical of basalts formed in arc settings, all Tsaybahe samples are characterized on a primitive mantle-normalized spider diagram by light rare earth element (LREE) and Th enrichment, and Nb and Ti depletion, (Figure 5a). However, the Tsaybahe volcanic rocks show distinctly less LREE enrichment than Late Triassic Stuhini basalts from the Iskut River (Zagorevski et al., 2012) and Dease Lake areas (Figure 5a–f).

### Stuhini Group

Souther (1971) included all Late Triassic volcanic and sedimentary rocks that lie above a Middle Triassic unconformity and below the Late Triassic Sinwa limestone in the Stuhini Group. In the Dease Lake area the Stuhini Group has been subdivided into six Late Triassic map units (Gabrielse, 1998; Logan et al., 2012b; Figure 2). From oldest to youngest these are as follows: unit 1, a basal volcaniclastic unit of mixed, massive to thickly bedded reworked volcanic rocks and rare aphyric basalt flows that generally fine upward into unit 2, a well-bedded section of sandstone-siltstone with Late Triassic bivalves. Units 1 and 2 are overlain by unit 3, a thick package of coarse plagioclase-phyric basalt and andesite flows, and subordinate clastic rocks, and unit 4, isolated, thin units of alkalic, sparse K-feldspar–phyric latite and maroon basalt. Unit 5 is composed of pyroxene±plagioclase–phyric monomict flow breccia and rare pillowed basalt that are interlayered within unit 6, an upper unit of massive volcaniclastic rocks containing plagioclase- and pyroxene-phyric basalt clasts. Four petrologically distinct suites of volcanic rocks are recognized within the Late Triassic Stuhini Group: aphyric basalt (lT̄Sv), plagioclase porphyry (lT̄Spp), latite porphyry (lT̄Smv) and pyroxene porphyry (lT̄Spx, Figure 2). The plagioclase and latite porphyries of units 3 and 4 respectively are mainly restricted to the medial stratigraphic position between reworked volcaniclastic rocks of units 2 and 5. The aphyric and pyroxene-phyric basalt suites are concentrated in the area south of Ross Creek (Logan et al., 2012c), within the upper volcaniclastic unit 6.

### Aphyric Basalt

Aphyric basalt and basaltic andesite flows occur throughout the massive, cliff-forming units of chaotic, nongraded, matrix-supported cobble to pebble volcanic conglomerate and associated volcanic sandstone that dominate the lower and uppermost parts of the Stuhini Group. The volcanic rocks include aphyric to sparsely plagioclase-phyric coherent flows, tuff breccia and lapilli tuff.

Four samples of aphyric flow and one sample of sparse plagioclase-phyric crystal tuff were collected for analyses. Two are from the area south of Ross Creek and two are from the upper volcaniclastic unit north of the Tanzilla River at

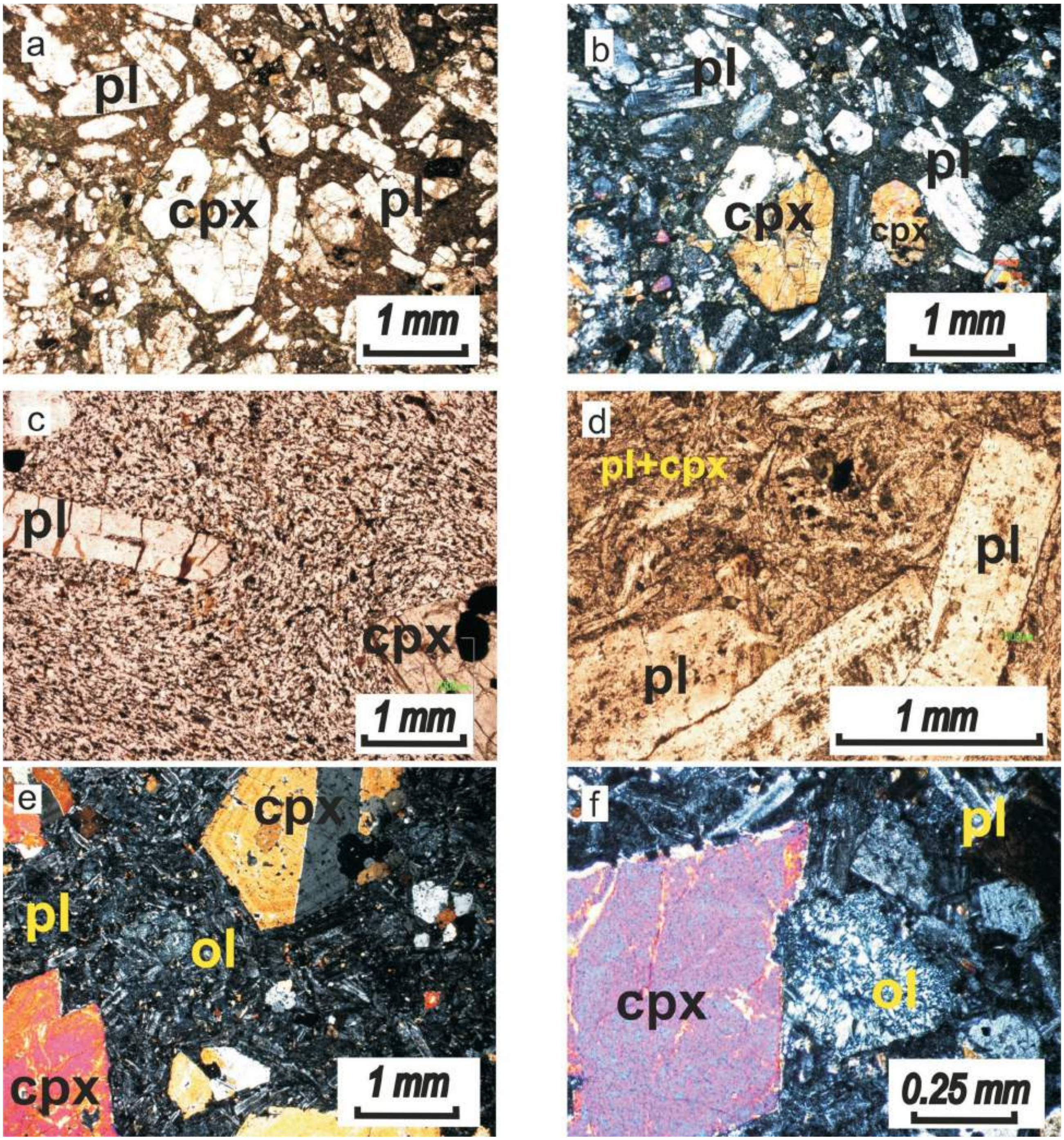


**Figure 3.** Photomicrographs of Middle Triassic, Late Triassic and Early to Middle Jurassic volcanic units: **a)** Tsaybahe crowded augite-plagioclase–phyric basalt breccia, plane-polarized light; **b)** crossed nicols; **c)** Stuhini sparse plagioclase-phyric andesite; **d)** Stuhini crowded plagioclase-phyric basalt; **e)** Hazelton pyroxene-phyric basalt with twinned and oscillatory zoned inclusion-rich augite phenocrysts in plagioclase-pyroxene-olivine matrix (crossed nicols); **f)** detail of intergrown augite and olivine crystal in Hazelton pyroxene-phyric basalt (crossed nicols). Abbreviations: cpx, clinopyroxene; ol, olivine; pl, plagioclase.

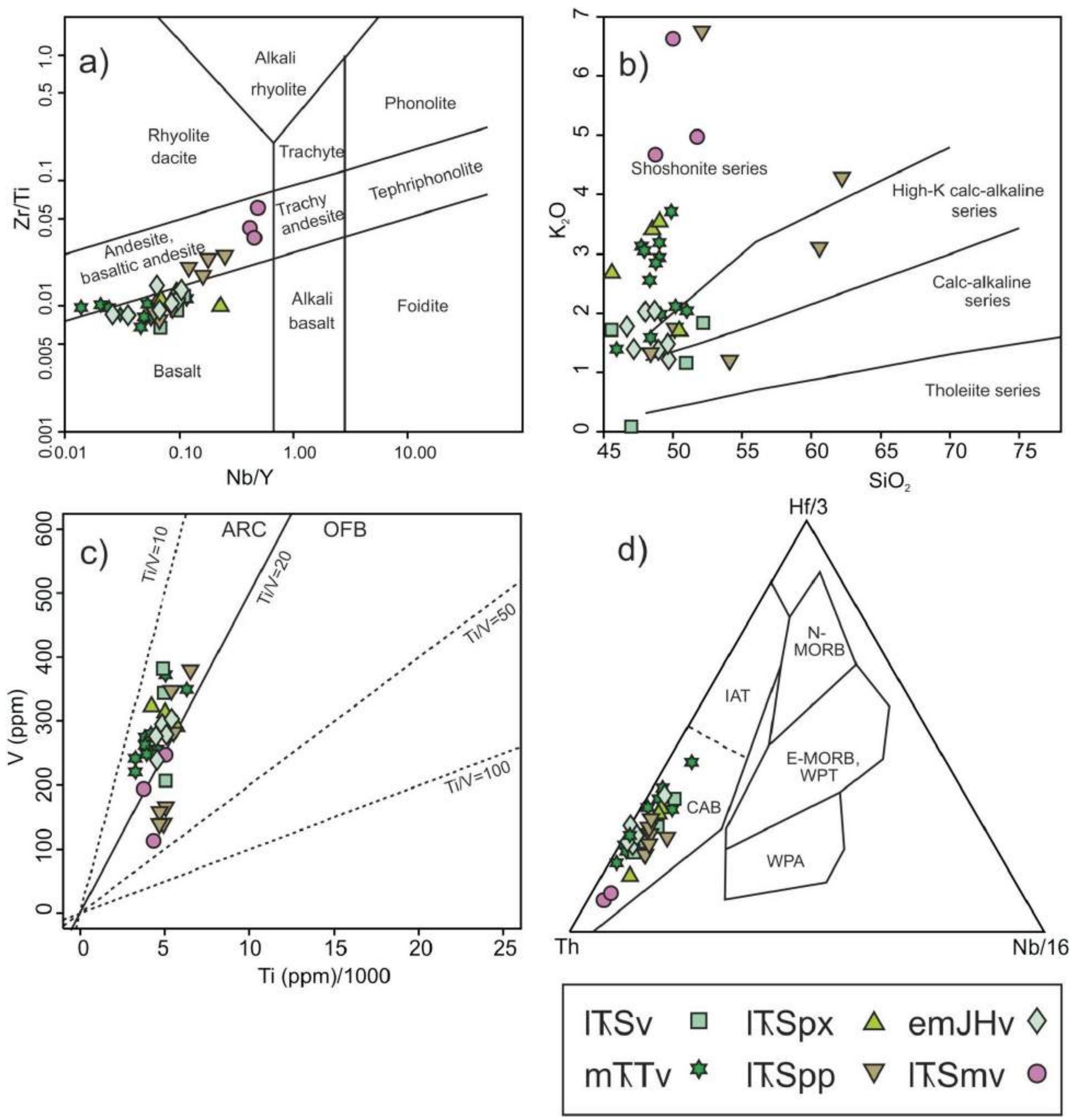


**Figure 4. a)** A Nb/Y vs. Zr/Ti classification diagram (Pearce, 1996) showing compositional range and classification for the Middle and Late Triassic and Early to Middle Jurassic basalt in the study area. **b)** Classification diagram based on $SiO_2$ vs. $K_2O$ (after Peccerillo and Taylor, 1976), used to distinguish shoshonitic, high-K calcalkaline, calcalkaline and tholeiitic series rocks. **c)** Tectonic discrimination diagram based on Ti vs. V (after Shervais, 1982), used to distinguish between arc and non-arc basalt. **d)** Tectonic discrimination diagram based on Th-Hf-Ta (after Wood, 1980), used to identify arc basalt (high Th/Ta) and theoretically distinguish between calcalkaline basalt, tholeiitic-arc basalt and non-arc basalts. Symbols: mTrTv, Middle Triassic Tsaybahe pyroxene-phyric basalt; lTrSv, Late Triassic Stuhini aphyric basalts; lTrSpp, Late Triassic Stuhini plagioclase-phyric basalt and andesite; lTrSmv, Late Triassic Stuhini latite porphyry; lTrSpx, Late Triassic Stuhini pyroxene-phyric basalt; emJHv, Early to Middle Jurassic Hazelton pyroxene-phyric basalt. Abbreviations: CAB, calcalkaline basalt; IAT, island arc tholeiite; E- and N-MORB, enriched and normal mid-ocean-ridge basalt; OFB, ocean floor basalt; WPA, within-plate alkaline basalts; WPT, within-plate tholeiites.

Tatsho Creek (Logan et al., 2012c). All plot in the subalkalic basalt field on the Zr/Ti versus Nb/Y classification diagram (Figure 4a) of Pearce (1996) and occupy either the shoshonite, high-K, calcalkaline or the tholeiite series fields on the $SiO_2$ versus $K_2O$ diagram (Figure 4b) of Peccerillo and Taylor (1976). All samples occupy the arc field (Shervais, 1982) and calcalkaline-arc basalt field (Wood, 1980) on tectonic discrimination diagrams (Figure 4c, d).

The aphyric volcanic samples are characterized by LREE and Th enrichment, and Nb and Ti depletion, characteristic of basalts formed in arc settings (Figure 5b). The primitive mantle-normalized trace-element profiles of the basalts

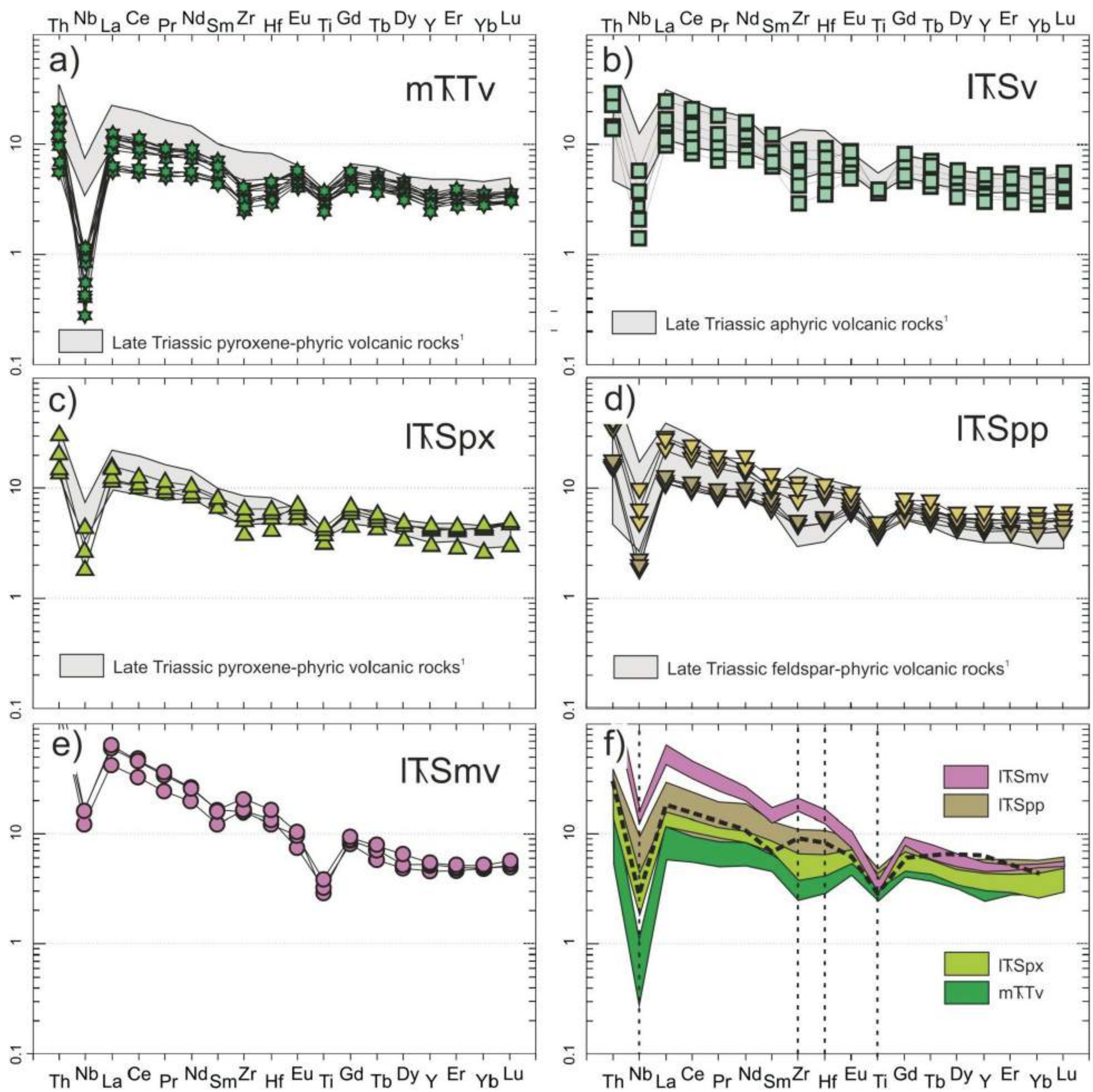


**Figure 5.** Primitive mantle-normalized (Sun and McDonough, 1989) extended trace-element profiles of Middle Triassic Tsaybahe and Late Triassic Stuhini Group volcanic rocks: **a)** Middle Triassic Tsaybahe pyroxene-phyric basalt; **b)–e)** Late Triassic Stuhini aphyric basalt, pyroxene-phyric basalt, plagioclase-phyric andesite (light green) and basalt (dark olive), and maroon latite; **f)** compares Tsaybahe pyroxene-phyric basalt, Stuhini pyroxene-phyric basalt, plagioclase-phyric basalt and maroon basalts with a typical calcalkaline island-arc basalt from the Sunda Arc (Jenner, 1996). Data source for comparison: [1] Zagorevski et al., 2012. Symbols: mT̄v, Middle Triassic Tsaybahe pyroxene-phyric basalt; lT̄Sv, Late Triassic Stuhini aphyric basalts; lT̄Spp, Late Triassic Stuhini plagioclase-phyric basalt and andesite; lT̄Smv, Late Triassic Stuhini latite porphyry; lT̄Spx, Late Triassic Stuhini pyroxene-phyric basalt.

overlap aphyric basalts assigned to the Stuhini Group in adjacent areas (Figure 5b, f; Zagorevski et al., 2012) and also overlap pyroxene- and plagioclase-phyric volcanic rocks from this study.

### Pyroxene Porphyry

Pyroxene-rich basalt flows, breccias and volcaniclastic rocks are the hallmark of the Stuhini Group in northwestern Stikinia (Souther, 1971, 1972; Anderson, 1993; Gabrielse, 1998; Logan et al., 2000), and these rock types are widely developed in the study area. Coherent pyroxene-phyric flow units are often complexly interlayered with coarse breccias dominated by pyroxene-phyric fragments and finer epiclastic units rich in pyroxene crystals; generally these units could not be mapped separately. Where distinguished, single flow units are commonly from 5 to 12 m thick, with massive interiors and flow-top breccias. Some flows contain subequal amounts of pyroxene and plagioclase phenocrysts, and others contain a much greater quantity of pyroxene than plagioclase phenocrysts. The former are characterized by typically quite small (~1–2 mm), subequal proportions of green or black pyroxene and white plagioclase laths in a fine-grained green groundmass. The pyroxene-phyric flows consist of typically 2–8 mm euhedral augite phenocrysts in a fine-grained green groundmass.

Three samples from massive flows (plus one duplicate) were collected from the area south of Ross Creek and northeast of the headwaters of Auguschidle Creek. They plot in the subalkalic basalt field on the Zr/Ti versus Nb/Y classification diagram (Figure 4a) of Pearce (1996). All plot as shoshonite or high-K calcalkaline series on the $SiO_2$ versus $K_2O$ diagram (Figure 4b; Peccerillo and Taylor, 1976) and in the arc field (Shervais, 1982) and calcalkaline-arc basalt field (Wood, 1980) on tectonic discrimination diagrams (Figure 4c, d). The Stuhini pyroxene±plagioclase porphyry samples are characterized by LREE and Th enrichment, and Nb and Ti depletion, characteristic of basalts formed in arc settings (Figure 5c). The primitive mantle-normalized trace-element profiles of the basalts overlap pyroxene-phyric basalts assigned to the Stuhini Group in adjacent areas (Figure 5c, f; Zagorevski et al., 2012).

### Plagioclase Porphyry

The plagioclase-phyric volcanic rocks of unit 3 comprise two suites: basaltic plagioclase-phyric flows occur south of the Tanzilla River and andesitic plagioclase-phyric flow rocks occupy isolated areas north of the Tanzilla River (Logan et al., 2012b, c). Both suites contain white- to cream-coloured, 2–8 mm euhedral plagioclase phenocrysts, sometimes glomeroporphyritic, in a fine-grained green groundmass. Intergrown fine plagioclase microlites and clinopyroxene form a pilotaxitic matrix, with sparse pyroxene phenocrysts present locally in the basaltic unit (Figure 3c, d). The plagioclase porphyry flows are generally coherent, unlike fragment-rich breccia deposits of the monolithic pyroxene porphyries. Immediately south of Ross Creek (Logan et al., 2012b, c) is a distinctive trachytic plagioclase-phyric andesite characterized by glassy 4–7 mm euhedral plagioclase crystals (5–7%) within a very fine grained dark groundmass that locally is glassy green and characterized by spherulitic devitrification textures.

Four of the eight samples plot in subalkalic basalt field and four in the andesite field on the Zr/Ti versus Nb/Y classification diagram (Figure 4a) of Pearce (1996). On an AFM diagram (not shown) the basalt samples are transitional tholeiitic to calcalkaline and the andesite calcalkaline. The andesite samples plot as shoshonite or high-K calcalkaline series, the basalts plot as high-K calcalkaline or calcalkaline series on the $SiO_2$ versus $K_2O$ diagram (Figure 4b; Peccerillo and Taylor, 1976). The plagioclase-phyric andesite has low vanadium abundances and Ti/V ratios and plot as non-arc basalts on Ti versus V diagram (Figure 4c; Shervais, 1982). These samples illustrate the problem of using this classification with calcalkaline lavas which commonly crystallize magnetite (strong affinity for V) leading to erroneous arc/non-arc designations. However, in the Zr versus Ti (Pearce and Cann, 1973, not shown) and Th-Hf-Nb (Wood, 1980) diagrams, which are unaffected by vanadium compatibility during calcalkaline basalt evolution, all plagioclase porphyry samples occupy calcalkaline arc basalt fields (Figure 4d).

The plagioclase porphyries are characterized by LREE and Th enrichment, and Nb and Ti depletion, characteristic of arc volcanism (Figure 5d). The primitive mantle-normalized trace-element profiles of the basalt are distinctly less enriched in LREE compared to the andesite and both overlap plagioclase-phyric basalts assigned to the Stuhini Group in adjacent areas (Figure 5d; Zagorevski et al., 2012).

### Latite Porphyry

Unit 4 of the Stuhini Group includes a distinctive package of salmon pink-weathering porphyritic latite, trachyte, maroon-weathering basalt and epiclastic rocks that crop out northwest of Hluey Lakes along the Hluey Lake service road adjacent to a pink-weathering syenite porphyry (Logan et al., 2012a, c). Samples were collected from a maroon-coloured basalt/latite with abundant calcite-filled vesicles, and phenocrysts of plagioclase, K-feldspar and biotite in an aphanitic groundmass that locally displays trachytic flow textures. It is uncertain whether the potassic character of these rocks is primary or can be attributed entirely to alteration from the adjacent syenite.

Chemical data for the maroon volcanic unit is under-represented (n=3) and suspect due to the substantial amounts of secondary alteration minerals visible in thin section (K-feldspar, hematite, carbonate, chlorite and quartz) and reflected in the high loss-on-ignition (LOI) values (Table 1).

The samples plot as subalkalic andesite to alkali basalt/ trachyte on the Zr/Ti versus Nb/Y classification diagram (Figure 4a) of Pearce (1996). All three samples plot as shoshonite on the $SiO_2$ versus $K_2O$ diagram (Peccerillo and Taylor, 1976) and in the calcalkaline arc basalt fields (Shervais, 1982; Wood, 1980) on tectonic discrimination diagrams (Figure 4b, c, d).

The primitive mantle-normalized extended trace-element plots for the maroon volcanic unit are characterized by LREE and Th enrichment, and Nb and Ti depletion, characteristic of arc volcanic rocks (Figure 5e). This unit has distinctly higher LREE abundances than any of the other mafic volcanic units studied, and also has elevated Zr and Hf values, implying either an evolved source or extensive liquid evolution (Münker et al., 2004).

### Hazelton Group

The Early to Middle Jurassic rocks exposed east of Gnat Pass are subdivided into five units (Anderson, 1983; Gabrielse, 1998; Iverson et al., 2012a, Figures 2, 3). Units 1–3 include 625 m of thin- or medium-bedded volcanic lithic arenite with pebble conglomerate, siltstone and siliceous ash tuff layers. Units 4 and 5 are monomict pyroxene-phyric basalt conglomerate and flow breccias. Five samples of basalt from the uppermost flow unit (unit 5 of Iverson et al., 2012a) and two samples of basaltic dikes cutting unit 3 sedimentary rocks (Iverson et al., 2012a, Figure 2) were analyzed. The basalt is a coarse pyroxene±plagioclase±olivine–phyric rock (Figure 3e, f) typically unaltered, but containing a lower greenschist-facies metamorphic assemblages of epidote, calcite, quartz and pyrite. It is dominated by euhedral, twinned and oscillatory-zoned inclusion-rich clinopyroxene phenocrysts within a finer grained groundmass of plagioclase laths, subhedral to anhedral olivine phenocrysts pseudomorphed by serpentine and chlorite, pyroxene and opaque minerals.

All Hazelton Group samples plot in the subalkalic basalt field on the Zr/Ti versus Nb/Y classification diagram (Figure 4a) of Pearce (1996) and cluster around the overlapping fields of shoshonite and high-K calcalkaline series at $SiO_2$ concentrations between 47–50 wt. % on the $SiO_2$ versus $K_2O$ diagram (Figure 4b) of Peccerillo and Taylor (1976). They plot in the arc field (Shervais, 1982) and calcalkaline-arc basalt field (Wood, 1980) on tectonic discrimination diagrams (Figure 4c, d) and are tholeiitic to transitional calcalkaline on the AFM diagram (Irvine and Baragar, 1971, not shown).

The Hazelton pyroxene porphyry samples are characterized by Th and LREE enrichment, and Nb and Ti depletion, characteristic of basalts formed in arc settings (Figure 6a). The trace-element profiles overlap pyroxene-phyric basalts assigned to the Stuhini Group in the study area and adjacent areas (Figure 6a).

## Discussion

The primitive mantle-normalized extended trace-element plots for the Middle Triassic, Late Triassic and Early to Middle Jurassic basalt samples all display LREE and Th enrichment, and Nb and Ti depletion, characteristic of calcalkaline basalts generated in an arc setting or derived from the subarc lithospheric mantle (Jenner, 1996; Figures 5, 6).

The normalized trace-element profiles for the LREEs (La, Ce, Pr, Nd) and middle rare earth elements (MREEs; Sm, Eu, Gd, Tb, Dy, Ho) for the Middle and Late Triassic basalts show progressive enrichment with progressively higher stratigraphic position and relatively younger ages (increasing $La/Sm_{NC}$; Table 2). The heavy rare earth element (HREE; Er, Tm, Yb, Lu) abundances overlap but conform to this same pattern. The normalized trace-element profiles for the Late Triassic basalts overlap Late Triassic aphyric, pyroxene-phyric and plagioclase-phyric basalts of the Stuhini Group in adjacent areas (Figure 5; Zagorevski et al., 2012). The relatively high concentration of $P_2O_5$ in the Tsaybahe pyroxene porphyries (approximately twice the average wt. % $P_2O_5$ of the other basalt units) is hard to reconcile with these being the most primitive type of basalt (i.e., highest MgO, Cr and Ni and lowest Y and Nb/Zr; Table 2).

The normalized trace-element profiles for the Hazelton basalts east of Gnat Pass overlap the profiles from Early Jurassic Cold Fish and Mount Brock basalts of the Hazelton Group (Figure 6b) in the adjacent Spatsizi map area (104H; Evenchick and Thorkelson, 2005) but not the profiles from rift basalts of the Early to Middle Jurassic Willow Ridge Complex (Figure 6c) in the Telegraph Creek map area (104G; Barresi and Dostal, 2005). The Willow Ridge Complex comprises a bimodal suite of basalt, basaltic andesite and rhyolite, which spans the Toarcian-Aalenian boundary (Early Jurassic to Middle Jurassic) and is age-equivalent to the host rocks at Eskay Creek (Alldrick et al., 2004). Primitive mantle-normalized trace-element abundance patterns for the mafic rocks from the Willow Ridge Complex show a slight enrichment of LREEs sloping from Th to Sm and a slight negative Nb anomaly (Barresi and Dostal, 2005).

The primitive mantle-normalized extended trace-element plots for the Hazelton basalt also overlap the plots for intrusive rocks of the age-equivalent Middle Jurassic Three Sisters pluton (van Straaten et al., 2012b), but more precisely match the trace-element pattern for hornblende-augite gabbro of the Late Triassic Beggerlay Creek pluton (van Straaten et al., 2012b; Figure 6d). The relative abundances and trace-element patterns of the Hazelton basalt also overlap those of Late Triassic pyroxene-phyric basalt from the study area and the Iskut River area (Figure 6a; Zagorevski et al., 2012), suggesting that successive Mesozoic arc mag-

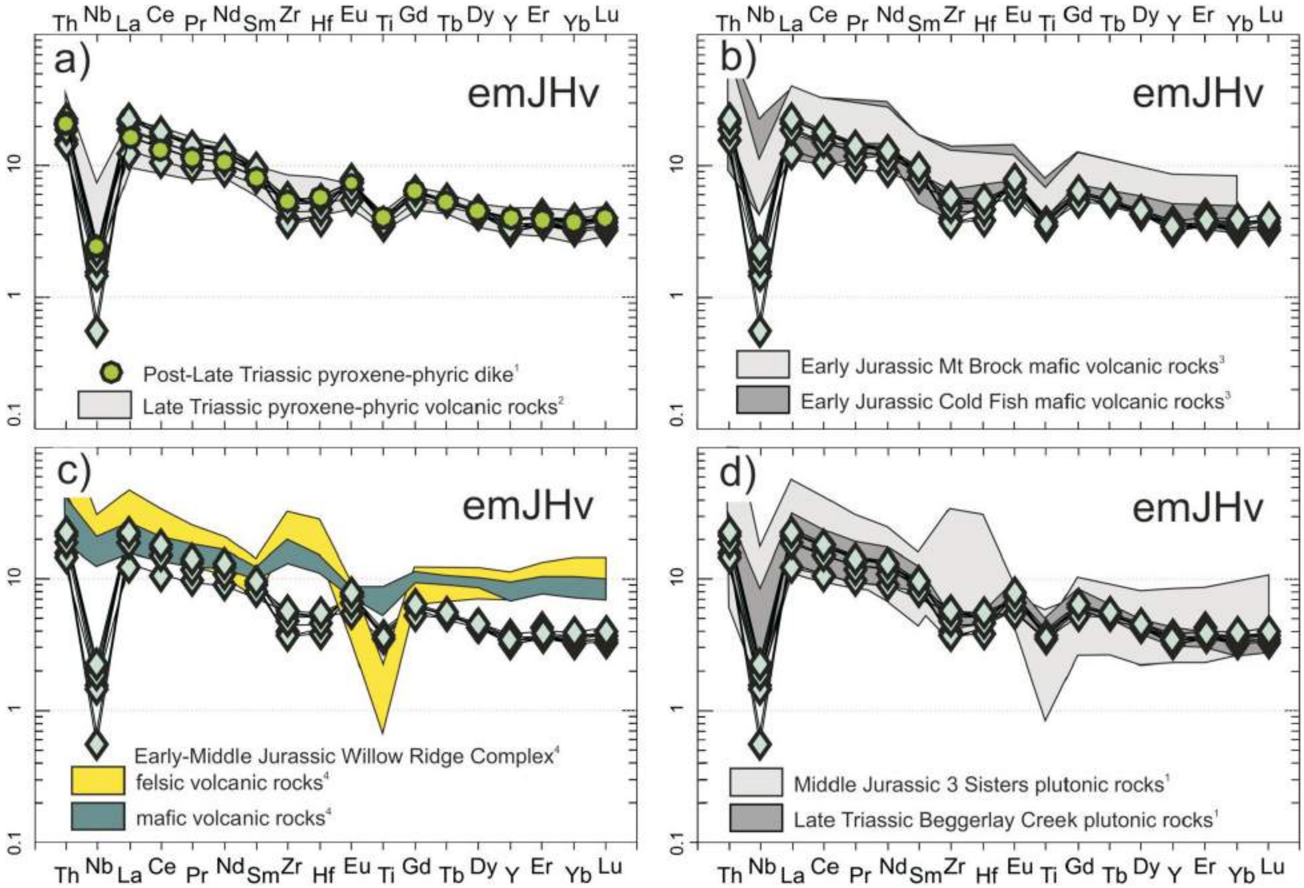


**Figure 6.** Primitive mantle-normalized (Sun and McDonough, 1989) extended trace-element profiles of Early to Middle Jurassic Hazelton Group pyroxene-phyric basalt. Data sources for comparison: [1] van Straaten et al. (2012b); [2] Zagorevski et al. (2012), plus analyses from this study; [3] Evenchick and Thorkelson (2005); [4] Barresi and Dostal (2005). Symbol: emJHv, Early to Middle Jurassic Hazelton pyroxene porphyry.

mas were likely generated from similar subduction-modified mantle and erupted rapidly with relatively short residence time in the upper crust to prevent substantial fractionation or assimilation of more felsic material. In addition, a post–Late Triassic pyroxene-phyric dike that cuts the ca. 221 Ma Cake Hill pluton (Anderson and Bevier, 1992; van Straaten et al., 2012a) has an identical primitive mantle-normalized trace-element pattern as the Hazelton basalt, suggesting it may represent a feeder dike to the overlying Hazelton Group volcanic rocks (Figure 6a).

## Alteration Guides for Exploration

Major element mobility of $K_2O$, $Na_2O$ and CaO during even low-grade alteration is well established (Davies et al., 1979) and, in areas peripheral to magmatic centres, understanding element mobility can provide exploration vectors within hydrothermal alteration zones (Barrett and MacLean, 1993). The latite porphyry and plagioclase-phyric andesite suites of the Stuhini Group are characterized by elevated $K_2O$ and/or $Na_2O$ related to secondary alteration. The latite porphyry samples have high LOI values, mobile low field strength elements (LFSEs) including Th, and are located adjacent to a potassic intrusive centre and Cu-Au prospect (MINFILE 104J 013; BC Geological Survey, 2012). However, alteration in the plagioclase-phyric andesite samples is more subtle, with only slightly elevated LOI values and no nearby intrusion or geophysical expression

**Table 2.** Selected element concentrations and ratios for the Middle Triassic, Late Triassic and Early to Middle Jurassic basalts collected from the area covered by the Dease Lake (104J) and Cry Lake (104I) map sheets, northwestern British Columbia.

| Unit[1] | $La/Sm_{NC}$ | $La/Sm_{NC}$[2] | $P_2O_5$[2] (wt %) | Ni/Cr[2] | Y[2] (ppm) | Nb/Zr[2] |
|---|---|---|---|---|---|---|
| emJHv | 1.80–2.65 | 2.32 | 0.29 | 0.172 | 15.4 | 0.02 |
| lTRSmv | 3.42–3.81 | 3.42 | 0.33 | 0.375 | 22.2 | 0.04 |
| lTRSpp | 1.52–2.62 | 2.04 | 0.3 | 0.417 | 21.5 | 0.04 |
| lTRSv | 1.53–2.18 | 1.77 | 0.25 | 0.376 | 17.3 | 0.03 |
| lTRSpx | 1.46–2.26 | 1.69 | 0.34 | 0.387 | 19.2 | 0.02 |
| mTRTv | 1.33–2.12 | 1.59 | 0.52 | 0.269 | 13.2 | 0.01 |

[1] Unit: mTRTv, Middle Triassic Tsaybahe pyroxene-phyric basalt; lTRSv, Late Triassic Stuhini aphyric basalts; lTRSpp, Late Triassic Stuhini plagioclase-phyric basalt and andesite; lTRSmv, Late Triassic Stuhini latite porphyry; lTRSpx, Late Triassic Stuhini pyroxene-phyric basalt; emJHv, Early to Middle Jurassic Hazelton pyroxene porphyry

[2] Average values

Abbreviation: NC, chondrite normalized

(Aeroquest Airborne, 2012) indicative of a buried intrusion in the area. Regional geochemical data (Jackaman, 2012) for the area south of Ross Creek, where three of the four plagioclase-phyric andesite samples originate, indicate two streams draining the area with anomalous copper values (within the 95$^{th}$ percentile) that warrant follow-up.

## Conclusions

Middle Triassic, Late Triassic and Early to Middle Jurassic pyroxene-phyric volcanic rocks occur in northern Stikinia (Brown et al., 1992; Gabrielse, 1998; Iverson et al., 2012a). In this study, they have similar physical characteristics, mineralogy and chemistry, which make them difficult to distinguish from one another without independent age constraints. They have primitive mantle-normalized extended trace-element patterns that display LREE and Th enrichment, and Nb and Ti depletion, characteristic of calcalkaline basalts generated in an arc setting. These geochemical patterns overlap those from correlative units in adjacent areas (Evenchick and Thorkelson, 2005; Zagorevski et al., 2012) and are also similar to those from Late Triassic and Middle Jurassic calcalkaline plutonic suites in the region (van Straaten et al., 2012b).

The Early to Middle Jurassic pyroxene-phyric rocks of the Hazelton Group east of Gnat Pass are the same age as the Willow Ridge Complex (Alldrick et al., 2004) and the basalts of the Salmon River Formation (Anderson and Thorkelson, 1990) at Eskay Creek. However, the basalts at Eskay Creek have a tholeiitic, N-MORB signature (Barrett and Sherlock, 1996), which is different from the calcalkaline, arc signature of the volcanic rocks east of Gnat Pass.

## Acknowledgements

Geoscience BC provided financial and logistical support for the field collection of samples in 2011 and follow-up analyses in 2012. Many thanks to C. Sluggett for cheerfully and efficiently managing the project. This paper was substantially improved through review by P. Schiarizza.

## References

Aeroquest Airborne (2012): Report on a helicopter-borne magnetic survey (Aeroquest Job #11-046) for Geoscience BC; Geoscience BC, Report 2012-2, 11 p.

Allen, D.G., Panteleyev, A. and Armstrong, A.T. (1976): Galore Creek; *in* Porphyry Deposits of the Canadian Cordillera, A. Sutherland Brown, (ed.), Canadian Institute of Mining and Metallurgy, Special Volume 15, p. 402–414.

Alldrick, D.J., Stewart, M.L., Nelson, J.L. and Simpson, K.A. (2004): Tracking the Eskay Rift through northern British Columbia—geology and mineral occurrences of the upper Iskut River area; BC Ministry of Energy, Mines and Natural Gas, Geological Fieldwork 2003, Paper 2004-01, p. 1–18.

Anderson, R.G. (1983): Geology of the Hotailuh batholith and surrounding volcanic and sedimentary rocks, north-central British Columbia; Carleton University, Ottawa, Ph.D. thesis, 669 p.

Anderson, R.G. (1984): Late Triassic and Jurassic magmatism along the Stikine Arch and the geology of the Stikine batholith, north-central British Columbia; *in* Current Research, Part A, Geological Survey of Canada, Paper 84-1A, p. 67–73.

Anderson, R.G. (1993): A Mesozoic stratigraphic and plutonic framework for northwestern Stikinia (Iskut River area), northwestern British Columbia; *in* Mesozoic Paleogeography of the Western United States, II: Los Angeles, CA, G. Dunne and K. McDougall (ed.), Society of Economic Paleontologists and Mineralogists, Pacific Section, p. 477–494.

Anderson, R.G. and Bevier, M.L. (1992): New Late Triassic and Early Jurassic U-Pb zircon ages from the Hotailuh batholith, Cry Lake map area, north-central British Columbia; *in* Radiogenic Age and Isotope Studies, Report 6, Geological Survey of Canada, Paper 92-2, p. 145–152.

Anderson, R.G. and Thorkelson, D.J. (1990): Mesozoic stratigraphy and setting for some mineral deposits in Iskut River map area, northwestern British Columbia; *in* Current Research, Part E, Geological Survey of Canada, Paper 90-1E, p. 131–139.

Barr, D.A., Fox, P.E., Northcote, K.E. and Preto, V.A. (1976): The alkaline suite porphyry deposits: a summary; *in* Porphyry Deposits of the Canadian Cordillera, A. Sutherland Brown (ed.), Canadian Institute of Mining and Metallurgy, Special Volume 15, p. 359–367.

Barresi, T. and Dostal, J. (2005): Geochemistry and petrography of Upper Hazelton Group volcanics: VHMS-favourable stratigraphy in the Iskut River and Telegraph Creek map areas, northwestern British Columbia; *in* Geological Fieldwork 2004, BC Ministry of Energy, Mines and Natural Gas, Paper 2005-01, p. 39–47.

Barrett, T.J. and MacLean, W.H. (1994): Chemostratigraphy and hydrothermal alteration in exploration for VHMS deposits in greenstones and younger volcanic rocks; *in* Alteration and Alteration Processes associated with Ore-forming Systems, D.R. Lentz (ed.), Geological Association of Canada, Short Course Notes, v. 11, p. 433–467.

Barrett, T.J. and Sherlock, R.L. (1996): Geology, lithogeochemistry and volcanic setting of the Eskay Creek Au-Ag-Cu-Zn deposit, northwestern British Columbia; Exploration and Mining Geology, v. 5, p. 339–368.

BC Geological Survey, (2012): MINFILE BC mineral deposits database; BC Ministry of Energy, Mines and Natural Gas <http://minfile.ca/> [November 2012].

Brown, D.A., Greig, C.J., Bevier, M.L. and McClelland, W.C. (1992): U-Pb zircon ages for the Hazelton Group and Cone Mountain and Limpoke plutons, Telegraph Creek map area, northwestern British Columbia: age constraints on volcanism and deformation; *in* Radiogenic Age and Isotopic Studies, Report 6; Geological Survey of Canada, Paper 92-2, p. 153–162.

Brown, D.A., Gunning, M.H. and Greig, C.J. (1996): The Stikine Project: geology of Western Telegraph Creek map area, northwestern British Columbia; BC Ministry of Energy, Mines and Natural Gas, Bulletin 95, 175 p.

Davies, J.F., Grant, R.W.E. and Whitehead, R.E.S. (1979): Immobile trace elements and Archean volcanic stratigraphy in the Timmins mining area, Ontario; Canadian Journal of Earth Sciences, v 16, p. 305–311.

Evenchick, C.A. and Thorkelson, D.J. (2005): Geology of the Spatsizi River map area, north-central British Columbia; Geological Survey of Canada, Bulletin 577, 189 p.

Fox, P.E. (1975): Alkaline rocks and related mineral deposits of the Quesnel Trough, British Columbia, Cordilleran Section; Geological Association of Canada, Symposium on Intrusive Rocks and Related Mineralization of the Canadian Cordillera, Program and Abstracts, p. 12.

Gabrielse, H. (1998): Geology of Cry Lake and Dease Lake map areas, north-central British Columbia; Geological Survey of Canada, Bulletin 4, 118 p.

Govindaraju, (1994): 1994 compilation of working values and sample description for 383 geostandards; Geostandards Newsletter, v. 18, issue S1, p. 1–158.

Henderson, C.M. and Perry, D.G. (1981): A Lower Jurassic heteroporid bryozoan and associated biota, Turnagain Lake, British Columbia; Canadian Journal of Earth Sciences, v. 18, p. 457–468.

Irvine, T.N. and Baragar, W.R. (1971): A guide to the chemical classification of the common volcanic rocks; Canadian Journal of Earth Sciences, v. 8, p. 523–548.

Iverson, O., Mahoney, J.B. and Logan, J.M. (2012a): Dease Lake Geoscience Project, Part IV: Tsaybahe group: lithological and geochemical characterization of Middle Triassic volcanism in the Stikine Arch, north-central British Columbia; *in* BC Ministry of Energy, Mines and Natural Gas, Geological Fieldwork 2011, Report 2012-1, p. 17–22, URL <http://www.empr.gov.bc.ca/Mining/Geoscience/PublicationsCatalogue/Fieldwork/Documents/2011/03_Iverson_2011.pdf> [November 2012].

Iverson, O., Mahoney, J.B. and Logan, J.M. (2012b): Reassessment of Triassic and Jurassic volcanic strata in the Dease Lake region, northern British Columbia; Geological Association of Canada, Pacific Section, Cordilleran Tectonics Workshop 2012, Victoria British Columbia, poster.

Jackaman, W. (2012): QUEST-Northwest Project: new regional geochemical survey and sample reanalysis data (NTS 104F, G, H, I, J), northern British Columbia; *in* Geoscience BC Summary of Activities 2011, Report 2012-1, p. 15–18, URL <http://www.geosciencebc.com/i/pdf/SummaryofActivities2011/SoA2011_Jackaman.pdf> [October 2012].

Jenner, G.A. (1996): Trace element geochemistry of igneous rocks: geochemical nomenclature and analytical geochemistry; *in* Trace Element Geochemistry of Volcanic Rocks: Applications for Massive Sulfide Exploration, D.A. Wyman (ed.), Geological Association of Canada, Short Course Notes, v. 12, p. 51–77.

Logan, J.M. and Bath, A.B. (2006): Geochemistry of Nicola Group basalt from the central Quesnel Trough at the Latitude of Mount Polley (NTS 093A/5, 6, 11, 12), central British Columbia; *in* BC Ministry of Energy, Mines and Natural Gas, Geological Fieldwork 2005, Report 2006-1, p. 83–98, URL<http://www.empr.gov.bc.ca/Mining/Geoscience/PublicationsCatalogue/Fieldwork/Documents/2005/Paper09.pdf> [November 2012].

Logan, J.M., Drobe, J.R. and McClelland, W.C. (2000): Geology of the Forrest Kerr-Mess Creek area, northwestern British Columbia (NTS 104B/10, 15 & 104G/2 & 7W); BC Ministry of Energy, Mines and Natural Gas, Bulletin 104, 132 p.

Logan, J.M., Diakow, L.J., van Straaten, B.I., Moynihan, D.P. and Iverson, O. (2012a): QUEST-Northwest Mapping, BC Geological Survey Dease Lake Geoscience Project, northern British Columbia; *in* Geoscience BC, Summary of Activities 2011, Report 2012-1 p. 5–14, URL <http://www.geosciencebc.com/i/pdf/SummaryofActivities2011/SoA2011_Logan.pdf> [November 2012].

Logan, J.M., Moynihan, D.P. and Diakow, L.J. (2012b): Dease Lake Geoscience Project, Part I: Geology and mineralization of the Dease Lake (104J/8) and east-half of the Little Tuya River (104J/7E) map sheets, northern British Columbia; *in* Geological Fieldwork 2011, BC Ministry of Energy, Mines and Natural Gas, Geological Fieldwork 2011, Report 2012-1, p. 23–44, URL <http://www.empr.gov.bc.ca/Mining/Geoscience/PublicationsCatalogue/Fieldwork/Documents/2011/04_Logan_2011.pdf> [November 2012].

Logan, J.M., Moynihan, D.P., Diakow, L.J. and Van Straaten, B.I. (2012c): Dease Lake - Little Tuya River Geology, NTS 104J/ 08 & 07E; Geoscience BC Map 2012-08-1 and BC Ministry of Energy, Mines and Natural Gas, Open File Map 2012-04, 1:50 000 scale.

Lueck, B.A. and Russell, J.K. (1994): Silica-undersaturated, zoned alkaline intrusions within the British Columbia cordillera; *in* Geological Fieldwork 1993, BC Ministry of Energy, Mines and Natural Gas, Paper 1994-1, p. 311–315.

Marsden, H. and Thorkelson, D.J. (1992): Geology of the Hazelton volcanic belt in British Columbia: implications for the Early to Middle Jurassic evolution of Stikinia; Tectonics, v. 11 (6), p. 1266–1287.

Massey, N.W.D., MacIntyre, D.G., Desjardins, P.J. and Cooney, R.T. (2005): Digital geology map of British Columbia: whole province; BC Ministry of Energy, Mines and Natural Gas, GeoFile 2005-1.

Moynihan, D.P. and Logan, J.M. (2012): Age, emplacement and mineralization of the Cretaceous Snow Peak pluton; *in* Geological Fieldwork 2011, BC Ministry of Energy, Mines and Natural Gas, Paper 2012-1, p. 69–74.

Münker, C., Wömer, G., Yogodzinski, G. and Churikova, T. (2004): Behaviour of high field strength elements in subduction zones: constraints from Kamchatka-Aleutian arc lavas; Earth and Planetary Science Letters, v. 224, p. 275–293.

Panteleyev, A., Bailey, D.G., Bloodgood, M.A. and Hancock, K.D. (1996): Geology and mineral deposits of the Quesnel River–Horse fly map area, central Quesnel Trough, British Columbia (NTS 93A/5, 6, 7, 11, 12, 13; 93B/9, 16; 93G/1; 93H/4); BC Ministry of Energy, Mines and Natural Gas, Bulletin 97, p. 156.

Pearce, J.A. and Cann, J.R. (1973): Tectonic setting of basic volcanic rocks determined using trace element analyses; Earth and Planetary Science Letters, v. 19, p. 290–300.

Peccerillo, A. and Taylor, S.R. (1976): Geochemistry of Eocene calc-alkaline volcanic rocks from the Kastamonu area, northern Turkey; Contribution to Mineralogy and Petrology, v. 58, p. 63–81.

Read, P.B. (1983): Geology, Classy Creek (104J/2E) and Stikine Canyon (104J/1W), British Columbia; Geological Survey of Canada, Open File Map 940, 1:50 000 scale.

Read, P.B. (1984): Geology, Klastine River (104G/16E), Ealue Lake (104H/13W), Cake Hill (104I/4W) and Stikine Canyon (104J/1E), British Columbia; Geological Survey of Canada, Open File Map 1080, 1:50 000 scale.

Read, P.B. and Psutka, J.F. (1990): Geology, Ealue Lake east-half (104H/13E) and Cullivan Creek (104H/14) map areas, British Columbia; Geological Survey of Canada, Open File Map 2241, 1:50 000 scale.

Scott, J.E., Richards, J.P., Heaman, L.M., Creaser, R.A. and Salazar, G.S. (2008): The Schaft Creek porphyry Cu-Mo-(Au) deposit, northwestern British Columbia; Exploration and Mining Geology, v. 17, p. 163–196.

Shervais, J.W. (1982): Ti-V plots and the petrogenesis of modern and ophiolitic lavas; Earth and Planetary Science Letters, v. 59, p. 101–118.

Simpson, K.A. (2012): QUEST-Northwest: Geoscience BC's new minerals project in northwest British Columbia (104G, 104J, parts of NTS 104A, B, F, H, I, K, 103O, P); *in* Geoscience BC, Summary of Activities 2011, Report 2012-1, p. 1–4. URL <http://www.geosciencebc.com/i/pdf/SummaryofActivities2011/SoA2011_Simpson.pdf> [November 2012].

Souther, J.G. (1971): Geology and mineral deposits of Tulsequah map-area, British Columbia; Geological Survey of Canada, Memoir 362, p. 76.

Souther, J.G. (1972): Telegraph Creek map area, British Columbia; Geological Survey of Canada, Paper 71-44, p. 38.

Sun, S.-s. and McDonough, W.F. (1989): Chemical and isotopic systematics of oceanic basalts: implications for mantle composition and processes; *in* Magmatism in the Ocean Basins, A.D. Saunders and M.J. Norry (ed.), Geological Society Special Publication 42, p. 313–345.

van Straaten, B.I., Logan, J.M. and Diakow, L.J. (2012a): Dease Lake Geoscience Project, Part II: preliminary report on the Mesozoic magmatic history and metallogeny of the Hotailuh batholith and surrounding volcanic and sedimentary rocks; *in* Geological Fieldwork 2011, BC Ministry of Energy, Mines and Natural Gas, Report 2012-1, p. 99–120, URL <http://www.empr.gov.bc.ca/Mining/Geoscience/PublicationsCatalogue/Fieldwork/Documents/2011/08_van_Straaten_2011.pdf> [November 2012].

van Straaten, B.I., Logan, J.M. and Diakow, L.J. (2012b): Mesozoic magmatic history and metallogeny of the Hotailuh batholith (NWBC); BC Ministry of Energy, Mines and Natural Gas, GeoFile 2012-08 and Geoscience BC Map 2012-10-1, 1:50 000 scale.

Wood, D.A. (1980): The application of the Th-Hf-Ta diagram to problems of tectonomagmatic classification and to establishing the nature of crustal contamination of basaltic lavas of the British Tertiary volcanic province; Earth and Planetary Science Letters, v. 50, p. 11–30.

Woodsworth, G.J., Anderson, R.G. and Armstrong, R.L. (1991): Plutonic regimes; *in* Geology of the Cordilleran Orogen in Canada, H. Gabrielse and C.J. Yorath (ed.), Geological Survey of Canada, Geology of Canada, no. 4, p. 491–531.

Zagorevski, A., Mihalynuk, M.G. and Logan, J.M. (2012): Geochemical characteristics of Mississippian to Pliensbachian volcanic and hypabyssal rocks in the Hoodoo Mountain area (NTS104B/14E); *in* Geological Fieldwork 2012, BC Ministry of Energy, Mines and Natural Gas, Paper 2012-1, p. 121–134, URL <http://www.empr.gov.bc.ca/Mining/Geoscience/PublicationsCatalogue/Fieldwork/Documents/2011/09_Zagorevski_2011.pdf> [November 2012].